Author queries:

Q1: OK as edited here?
Q2: Please clarify reference.
Q3: OK as edited here? Or should this be ", and conclusions are drawn"?
Q4: OK as edited here?
Q5: OK as edited here?
Q6: "re" okay?
Q7: OK as edited here?
Q8: OK as edited here?
Q9: OK as edited here?
Q10: OK as edited here?
Q11: Please clarify the wording "is focus."
Q12: OK as edited here? Or "results of variations of"?
Q13: OK as edited here? Please clarify wording.
Q14: Check the URL for [11].
Q15: Update on [27]?
Q16: OK as edited here to make this a complete sentence?
Q17: OK to delete "pursue"? Was additional text intended?
Q18: OK as edited here?
Q19: Is the period within the final line in the equation below ok, or was this intended to be at the end of the line? A period at the end of the line was added during copyediting.
Q20: Please clarify the wording in the beginning part of this sentence.

SIAM J. Applied Dynamical Systems
Vol. 0, No. 0, pp. 1–38

Bifurcation of Limit Cycles from Boundary Equilibria in Impacting Hybrid Systems*

Hong Tang† and Alan Champneys†

Abstract. A semianalytical method is derived for finding the existence and stability of single-impact periodic orbits born in a boundary equilibrium bifurcation in a general n-dimensional impacting hybrid system. Known results are reproduced for planar systems and general formulae derived for three-dimensional (3D) systems. A numerical implementation of the method is illustrated for several 3D examples and for an 8D wing-flap model that shows coexistence of attractors. It is shown how the method can easily be embedded within numerical continuation, and some remarks are made about necessary and sufficient conditions in arbitrary dimensional systems.

Key words. impact, boundary equilibrium bifurcation, hybrid system, periodic orbit

MSC codes. 37G05, 37G35, 37M2, 70G60, 70K42, 93B18

DOI. 10.1137/23M1552292

1. Introduction.

Differential equations with nonsmooth components occur in various situations. They arise in mechanical systems with scenarios of dry friction [9], impact [12, 20], and freeplay due to abrasion [9]; they also arise in electronic circuits, biological systems, and control engineering (see, e.g., [7, 18]). A general framework for piecewise-smooth dynamical systems was introduced in the book [7], in which phase space is partitioned into regions of smooth dynamics separated by codimension-one switching manifolds. The degree of smoothness across each such boundary determines a class of dynamical systems—for example, piecewise-smooth continuous systems Filippov systems and impacting hybrid systems—which in turn lead to unique kinds of *discontinuity-induced bifurcations* (DIBs). See [2, 14] for an overview of recent developments. In this paper we shall focus on hybrid systems for which in the overall system **AQ1** there is a discrete reset map applied at each boundary.

The simplest kind of DIB corresponds to a so-called boundary equilibrium bifurcation (BEB), where, under variation of a parameter, an equilibrium of one of the smooth components of phase spaces approaches a switching manifold. At nearby parameter values, we may find a pseudoequilibrium, which is not an equilibrium of the free dynamics, but of the flow constrained to the boundary. Much progress on analysis of BEBs has been made in two-dimensional systems [8, 23, 24]. In the case of planar (Filippov) piecewise-linear systems, significant recent progress has been made by Carmona and collaborators [3, 4, 5] on the

*Received by the editors February 8, 2023; accepted for publication (in revised form) by V. Kirk July 28, 2023; published electronically DATE.
https://doi.org/10.1137/23M1552292
Funding: The work of the first author was supported by the University of Bristol and Chinese Scholarship Council joint studentship 202006120007.
†Department of Engineering Mathematics, University of Bristol, Bristol BS8 1TR, UK (hong.tang@bristol.ac.uk, A.R.Champneys@bristol.ac.uk).

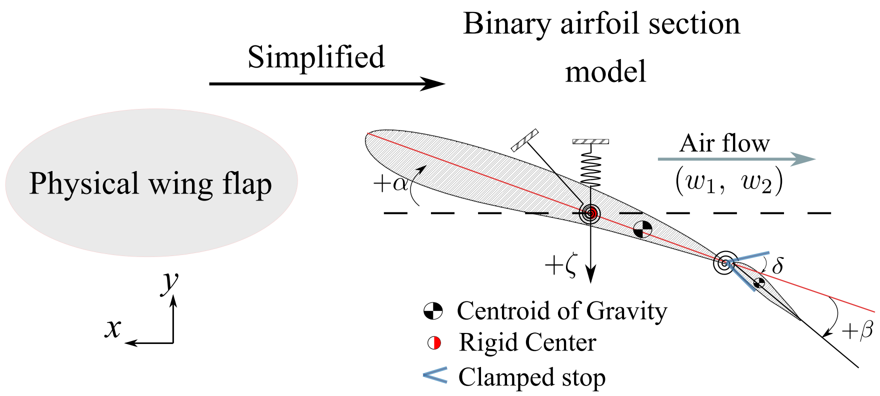

Figure 1. *Sketch of airfoil model; see the text for details.*

number of limit cycles that can coexist. A strict upper bound of 8 was found, which reduces to 1 in the absence of sliding. The particular unresolved question that we address in this paper regards BEBs in higher-dimensional systems. As we shall see, this is a difficult question in general, not least because there is no known general dimension-reduction method for piecewise-smooth systems [15]. Instead, we shall seek a semianalytic method that can trace curves of LCOs bifurcating at a BEB. Our work is motivated by the following example, which arose in our recent work on an eight-dimensional aircraft wing-flap model.

1.1. Motivating example. Some recent numerical results for a simplified airfoil model [27] are illustrated in Figure 1. Due to the rotary freeplay in the hinge between the flap and main body, such a system can be modelled as an impacting hybrid system, where a reset map is applied when the flap hits the stop. The equations of motion can be written in the form

$$\begin{cases} \dot{\mathbf{x}} = \mathbf{A}_{\mathrm{af}}(\bar{U})\mathbf{x} + \mathbf{G}(\bar{U}) \quad \text{for} \quad |x_3| < \delta, \\ \mathbf{x} = R(\mathbf{x}) \quad \text{for } |x_3| = \delta, \end{cases} \tag{1.1}$$

where $\mathbf{x} = [\zeta, \alpha, \beta, \dot{\zeta}, \dot{\alpha}, \dot{\beta}, w_1, w_2]^\top$, among which α and β measure the rotary pitch and flap motion, respectively, and ζ is the dimensionless heave motion. The parameter $\bar{U}$ is the dimensionless air velocity, and δ characterizes the amount of flap freeplay. The variables w_1 and w_2 are augmented variables that capture the so-called Theodorsen aerodynamic interactions [28]. The matrix $\mathbf{A}_{\mathrm{af}}$ specifies the dynamics of the airfoil when the flap is in freeplay. The reset map $R(\mathbf{x})$ is an affine map that maps the $\{|x_3^-| = \delta, \mathrm{sign}(x_3^-)\dot{x}_3^- > 0\}$ into $\{|x_3^+| = \delta, \mathrm{sign}(x_3^+)\dot{x}_3^+ < 0\}$ with a corresponding coefficient of restitution $0 < r < 1$ when projected onto the x_3 degree of freedom, $\dot{x}_3^+ = -r\dot{x}_3^-$. Full details of the model, including the coefficients of the matrix $\mathbf{A}_{\mathrm{af}}$, vector $\mathbf{G}$, and map R are given in Appendix A.

Figure 2(a) depicts a brute-force bifurcation diagram of stable limit states of (1.1) against flow velocity $\bar{U}$ for $\delta = 0.01$ rad and $r = 0.72$. Here we find that a stable equilibrium branch approaches the freeplay boundary at the critical value $\bar{U} = 0.64833$ and various attractors appear in sequence as $\bar{U}$ is increased further. Specifically, we find an initial BEB, where a stable LCO is born, which coexists with a stable pseudoequilibria branch, as shown in the zoomed-in Figure 2(b). Note how the amplitude of the LCO increases linearly with the

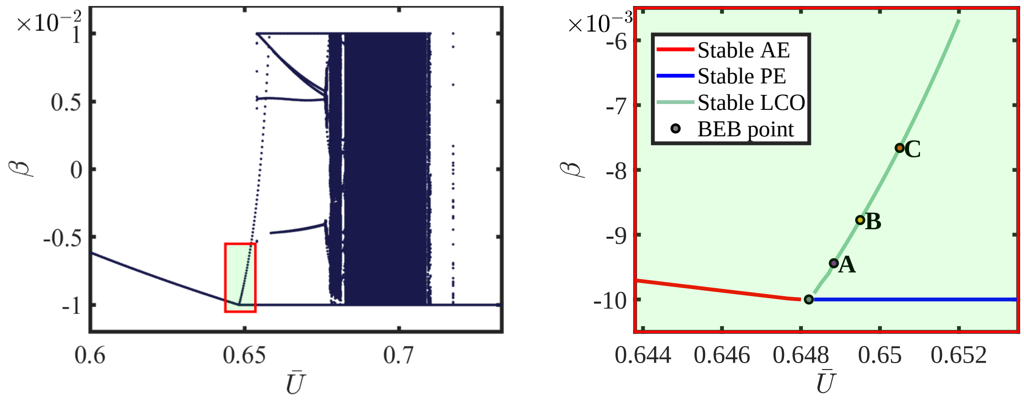

(a) (b)

Figure 2. *Brute force bifurcation diagram of the airfoil model* (1.1). (a) *The full bifurcation diagram capturing various dynamics.* (b) The *zoomed-in part of the first bifurcation from the boxed region in* (a): PE—*pseudoequilibria;* AE—*admissible equilibria. Full equations and parameter definitions are given in ??.* **AQ2**

variation of bifurcation parameter, as shown in Figure 3, which can be explained by existing theory [7, 8, 23, 24]. But what cannot be explained by the theory is how this table LCO coexists with a stable pseudoequilibrium. Thus, we require a genuinely multidimensional analysis.

1.2. Outline. The rest of the paper is organized as follows. Section 2 recalls how to construct a normal form at a BEB for an impacting hybrid system and summarizes what is known about classification of such bifurcations. In section 3 we derive a semianalytic method for constructing single-impact LCOs arising in such normal forms. Section 4 presents results from implementation of this algorithm; to reproduce (and extend) known examples in two dimensions, to attempt a general framework in three dimensions, and to explain the numerical observations in the wing-flap model. Some further analytical considerations are made in section 5, and a conclusion is drawn. **AQ3**

2. Preliminaries.

2.1. Impacting dynamical systems. Hybrid systems are characterized by the existence of both continuous and discrete dynamics. A parameter dependent *piecewise-smooth hybrid system* [7] is smooth in all regions, say, S_i, in phase space $\mathbb{R}^n$ that is partitioned by countably many codimension one manifolds Σ_{ij}, which can be defined as follows.

Definition 2.1. [7] *A* piecewise-smooth hybrid system *is composed of a set of ODEs*

$$\dot{\mathbf{x}} = F_i(\mathbf{x}, \mu) \quad \textit{for} \quad \mathbf{x} \in S_i,$$

plus a set of reset maps

$$\dot{\mathbf{x}} \mapsto R_{ij}(\mathbf{x}, \mu) \quad \textit{for} \quad \mathbf{x} \in \Sigma_{ij} := S_i \cap S_j,$$

where $\mathbf{x} \in \mathbb{R}^n$ *and* $\mu \in \mathbb{R}^m$. *Especially, an* impacting hybrid system *possesses* $R_{ij}(\mathbf{x}, \mu) : \Sigma_{ij} \to \Sigma_{ij}$, *and the flow is constrained locally to one side of the boundary.*

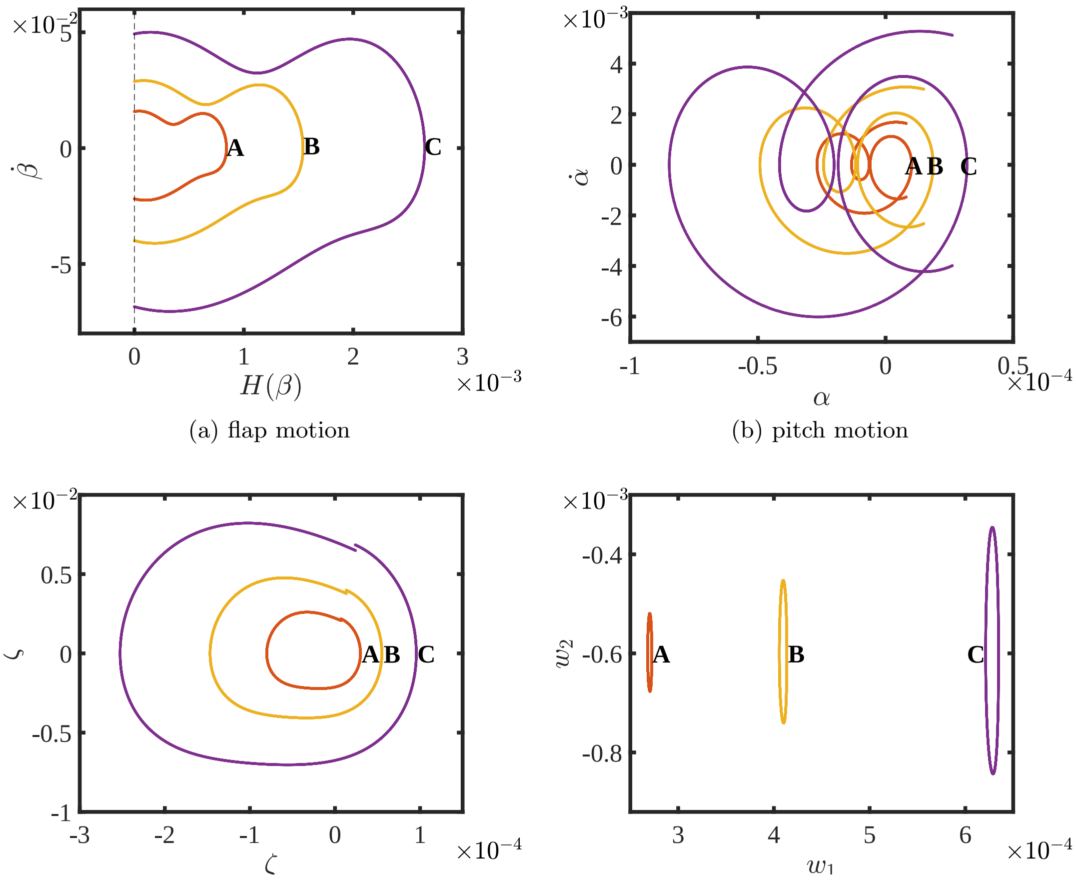

(a) flap motion (b) pitch motion

(c) heave motion (d) aerodynamic variables

Figure 3. *More details of the LCOs from Figure 2 at the points labelled A, B, and C; here $H(\beta)$ is a function (see Definition 2.1 and Theorem 2.4) to measure the state's distance from the impacting surface $\beta = -0.01$.*

Whenever the meaning is clear, we shall suppress the system's dependence on the parameter.

Because we are interested in DIBs involving a single-impact surface, it is worth simplifying notation by considering a local description in terms of a single-impacting surface Σ defined by a smooth function $H(\mathbf{x}) = 0$:

$$\Sigma = \{\mathbf{x} \mid H(\mathbf{x}) = 0\}, \quad \text{and the region governed by flow,} \quad S^+ = \{\mathbf{x} \mid H(\mathbf{x}) > 0\}.$$

Within this local description, we suppose that the dynamics is given by

$$\begin{cases} \dot{\mathbf{x}} = F(\mathbf{x}, \mu) & \text{for } H(\mathbf{x}) > 0, \\ \mathbf{x}^+ = R(\mathbf{x}^-) & \text{for } H(\mathbf{x}) = 0, \end{cases} \tag{2.1}$$

and we define an equilibrium of flow $F(\mathbf{x}, \mu)$ as $\mathbf{x}_0 = \mathbf{x}_0(\mu)$.

Within this context, it is also helpful to introduce some key concepts defined in [7, 21]. First, we let $v(\mathbf{x})$ and $a(\mathbf{x})$ be the normal velocity and acceleration, respectively, relative to the discontinuity surface, which can be defined using *Lie derivatives*:

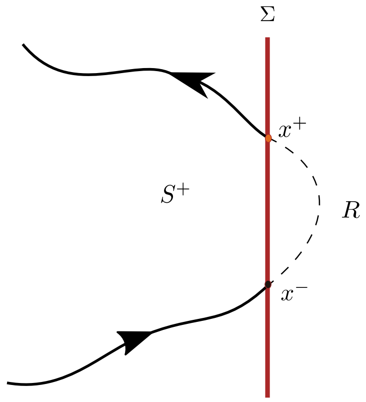

Figure 4. *An impacting hybrid system with a simple impact surface* Σ.

$$\begin{aligned} v(\mathbf{x}) &= \mathcal{L}_F(H)(\mathbf{x}) = \frac{dH}{dx}\dot{\mathbf{x}} = H_x F, \\ a(\mathbf{x}) &= \mathcal{L}_F^2(H)(\mathbf{x}) = H_{xx}F + H_x F_x F. \end{aligned} \tag{2.2}$$

The surface Σ can be partitioned depending on the sign of v: the *incoming set* $\Sigma^- = \{\mathbf{x} \in \Sigma : v(\mathbf{x}) < 0\}$, the *grazing set* $\Sigma^0 = \{\mathbf{x} \in \Sigma : v(\mathbf{x}) = 0\}$, and the *outgoing set* $\Sigma^+ = \{x \in \Sigma : v(x) > 0\}$. To define a well-posed impact law in the absence of friction, we need that it maps a grazing trajectory (where $v(\mathbf{x}) = 0$, $a(\mathbf{x}) > 0$) back to itself. Following [7], we can write the *reset map* in terms of a smooth function n-dimensional function $W(x)$, as follows:

$$\mathbf{x}^+ = R(\mathbf{x}^-) = \mathbf{x}^- + W(\mathbf{x}^-)v(\mathbf{x}^-). \tag{2.3}$$

Then we have

$$v^+ := v(\mathbf{x}^+) = (H_x F)_x R(\mathbf{x}^+) = [1 + (H_x F)_x W(\mathbf{x})]\ v(\mathbf{x}^-).$$

Furthermore, upon defining

$$r(\mathbf{x}) = -(1 + (H_x F)_x W(\mathbf{x}), \tag{2.4}$$

then r is an effective *coefficient of restitution,* and there is a physical constraint that $r > 0$ and $r < 1$ in order for the surface Σ_0 to be attracting.

If $0 < r < 1$ a trajectory v^+ will eventually become constrained to *sticking* (or *sliding*) on Σ^0, via *chattering,* an accumulation of impacts in finite time; see Figure 5. The *sticking subset* is defined as determined by

$$\Sigma^0_- = \{\mathbf{x} \in \Sigma^0 : a(\mathbf{x}) < 0\},$$

the stability of which is guaranteed if $0 < r < 1$ [8].

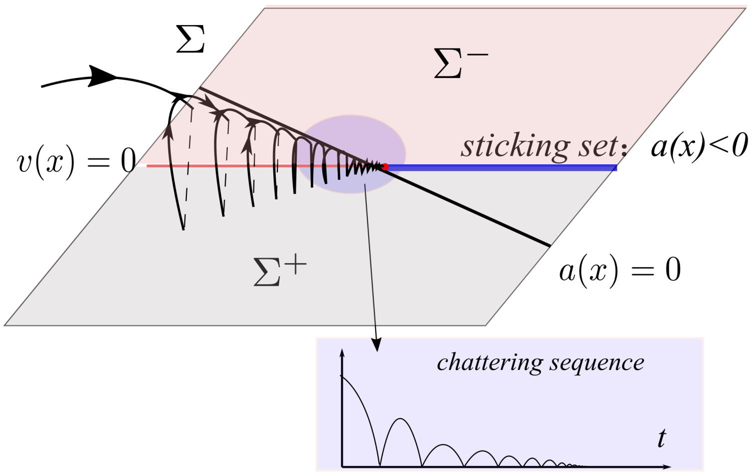

Figure 5. *Trajectory captured by Σ via chattering sequence.*

Theorem 2.2. *The stability of a sticking set is guaranteed if $0 < r < 1$ and $a(\mathbf{x}) < 0$.*

The dynamics in the sticking region can be defined by thinking of the impacting law as providing a normal force that keeps the motion on Σ. The dynamics within Σ_-^0 is determined by the sticking vector field [21], defined as

$$\dot{\mathbf{x}} = F_s = F(\mathbf{x}) - \lambda(\mathbf{x})W(\mathbf{x}), \quad \lambda(\mathbf{x}) > 0, \tag{2.5}$$

for a scalar $\lambda(\mathbf{x})$ which is defined as

$$H(\mathbf{x}(t)) \equiv 0, \tag{2.6a}$$

$$v(\mathbf{x}(t)) \equiv 0, \tag{2.6b}$$

$$\lambda(\mathbf{x}) = \frac{\mathcal{L}_F^2(H)(\mathbf{x})}{\mathcal{L}_W\mathcal{L}_F(H)(\mathbf{x})} = \frac{\mathcal{L}_F^2(H)(\mathbf{x})}{v_x W(\mathbf{x})} = \frac{-a(\mathbf{x})}{1 + r(\mathbf{x})}.$$

Note that $\lambda(\mathbf{x}) > 0$ if $0 < r < 1$ and $a(\mathbf{x}) < 0$. An explicit expression for sticking dynamics can then be obtained by eliminating λ in (2.5):

$$F_s = F - \frac{(H_{xx}F + H_x F_x)F}{(H_{xx}F + H_x F_x)W}W. \tag{2.7}$$

Following [7], we classify several different types of equilibria in (2.1).

Definition 2.3. *We call $\mathbf{x}_0$ satisfying $F(\mathbf{x}_0, \mu) = 0$ a* nominal *equilibrium, and further $\mathbf{x}_0$ is an* admissible *equilibrium of (2.1) if $H(\mathbf{x}_0) > 0$, a* boundary equilibrium *if $H(\mathbf{x}_0) = 0$, or a* virtual equilibrium *if $H(\mathbf{x}_0) < 0$.*

Moreover, $\mathbf{x}_0$ *is defined as a* pseudoequilibrium *(or a sliding equilibrium) if it is an equilibrium of the sticking vector field* (2.5) *for which*

$$F(\mathbf{x}_0) - \lambda W(\mathbf{x}_0) = 0, \quad H(\mathbf{x}_0) = 0.$$

Such pseudoequilibria are called virtual *when* $\lambda < 0$ *and* admissible *when* $\lambda > 0$.

2.2. Normal form for boundary equilibrium bifurcation. For simplicity, let us assume a system of the form (2.1) is dependent just on a single distinguished parameter μ, which AQ4 is true when $m = 1$ or in a codimension-one analysis though $m \geq 2$. Motivated by the example in Figures 2 and 3, we are interested in the situation where a stable *hyperbolic* admissible equilibrium $\mathbf{x}^*$ reaches the boundary $H(\mathbf{x}) = 0$ at some critical parameter value μ^*. Then, provided the matrix $\mathbf{A} = F_x(\mathbf{x}^*)$ is nonsingular and obeys other similar nondegeneracy conditions, it is argued in [8], by appealing to the Hartman–Grobman theorem, that the AQ5 dynamics of the system (2.1) sufficiently close to a BEB can be replaced by the following linearization at $\mathbf{x}^*, \mu^*$:

$$\begin{aligned} F(\mathbf{x}, \mu) &\approx \tilde{F}(\mathbf{x}, \mu) = \mathbf{A}(\mathbf{x} - \mathbf{x}^*) + \mathbf{M}(\mu - \mu^*), \\ H(\mathbf{x}, \mu) &\approx \tilde{H}(\mathbf{x}, \mu) = \mathbf{C}(\mathbf{x} - \mathbf{x}^*) + \mathbf{N}(\mu - \mu^*), \\ W(\mathbf{x}, \mu) &\approx \tilde{W}(\mathbf{x}^*, \mu^*) = -\mathbf{B}, \\ H(\mathbf{x}^*) &= 0. \end{aligned} \tag{2.8}$$

Moreover, the condition $\mathcal{L}_W(H)(\mathbf{x}) = 0$ can be rewritten as

$$\mathbf{CB} = 0, \tag{2.9}$$

where we emphasize that neither $\mathbf{B}$ nor $\mathbf{C}$ is zero vector, and the sliding vector field can be written locally as

$$F_s = \left(\mathbf{I} - \frac{\mathbf{BCA}}{\mathbf{CAB}}\right)(\mathbf{A}(\mathbf{x} - \mathbf{x}^*) + \mathbf{M}(\mu - \mu^*)).$$

Thus, the Jacobian of the sliding flow at point $\mathbf{x}^*$ is

$$\mathbf{A}_s = \left(\mathbf{I} - \frac{\mathbf{BCA}}{\mathbf{CAB}}\right)\mathbf{A}, \tag{2.10}$$

and with (2.4) the efficient restitution coefficient is rewritten as $r = \mathbf{CAB} - 1$. In particular, in what follows we shall assume the following nondegeneracy conditions:

$$\det(\mathbf{A}) \neq 0, \quad \mathbf{N} - \mathbf{CA}^{-1}\mathbf{M} \neq 0, \quad \mathbf{CA}^{-1}\mathbf{B} \neq 0. \tag{2.11}$$

In order to find the dynamics of (2.8)–(2.10), following [8], we can make further coordinate transformations to move the equilibrium to the origin and put any system undergoing a BEB into a normal form. For convenience, we collect together these transformations in the form of the following result, for which we give a constructive proof in Appendix B.

Theorem 2.4 (see [8]). *The linearized system* (2.8) *is scaling invariant, which means the same results will be obtained if* $\mathbf{x}-\mathbf{x}^*$ *and* $\mu-\mu^*$ *are multiplied by a* positive *scalar. Then, obeying the nondegeneracy condition* (2.11)*, to find the limit sets of* (2.1) *around* μ^* *is equivalent to finding these in the canonical linearized system*

$$\begin{cases} \dot{\mathbf{y}} = \hat{\mathbf{A}}\mathbf{y} & \text{for } H(\mathbf{y},\hat{\mu}) > 0 \text{ or } \mathbf{y} \in \Sigma^+ \cup \Sigma^0_+, \\ \dot{\mathbf{y}} = \hat{\mathbf{A}}_s\mathbf{y} & \text{for } \mathbf{y} \in \Sigma^0_-, \\ \mathbf{y} \mapsto \mathbf{P}\mathbf{y} & \text{for } \mathbf{y} \in \Sigma^-, \end{cases} \tag{2.12}$$

where, referring to the notation in (2.8)*, we define* $\mathbf{y} = \frac{\Delta\mathbf{x}+\mathbf{A}^{-1}\mathbf{M}\mu}{|\mu|(\mathbf{C}\mathbf{A}^{-1}\mathbf{M}-\mathbf{N})}$ *and*

$$\hat{\mu} = \frac{\mu}{|\mu|}, \quad H(\mathbf{y},\hat{\mu}) = \hat{\mathbf{C}}\mathbf{y} - \hat{\mu} = 0, \quad \hat{\mathbf{C}} = \mathbf{e}_1^\top, \quad \mathbf{P} = \mathbf{I} - \hat{\mathbf{B}}\hat{\mathbf{C}}\hat{\mathbf{A}}, \tag{2.13}$$

and matrices $\hat{\mathbf{A}}$*,* $\hat{\mathbf{A}}_s$*, and* $\hat{\mathbf{B}}$ *are related to the original* $\mathbf{A}$*,* $\mathbf{A}_s$*, and* $\mathbf{B}$*, respectively, by a* $\mathbf{C}$*-dependent coordinate transformation (see Appendix* B*). Moreover, the values of* $\hat{\mu} \in \{-1,0,1\}$ *are corresponding to pre-bifurcation, critical, and post-bifurcation values of the original bifurcation parameter* μ*.*

Note that within this normal form, a nominal equilibrium $\mathbf{y}_0 = \mathbf{0}$ of the flow in (2.12) is *admissible* if $\hat{\mu} = -1$ with $H(\mathbf{y}_0) > 0$, a *boundary equilibrium* if $\hat{\mu} = 0$ with and $H(\mathbf{y}_0) = 0$, or a *virtual equilibrium* if $\hat{\mu} = 1$ with $H(\mathbf{y}_0) < 0$. Moreover, to distinguish from $\mathbf{y}_0$, we denote $\hat{\mathbf{y}}_0$ a *pseudoequilibrium* (sliding equilibrium) if satisfying $F(\hat{\mathbf{y}}_0) - \tilde{\lambda}W(\hat{\mathbf{y}}_0) = 0$, $H(\hat{\mathbf{y}}_0) = 0$, and it is *virtual* when $\tilde{\lambda} < 0$ and *admissible* when $\tilde{\lambda} > 0$. For the case of a pseudoequilibrium we have

$$\begin{bmatrix} \hat{\mathbf{C}} \\ \hat{\mathbf{C}}\hat{\mathbf{A}} \\ \hat{\mathbf{A}}_s \end{bmatrix} \hat{\mathbf{y}}_0 = \begin{bmatrix} 1 \\ 0 \\ \mathbf{0}_{n\times 1} \end{bmatrix}, \tag{2.14}$$

which is formally well-posed because $\hat{\mathbf{A}}_s$ has rank $n-2$.

2.3. Equilibrium transitions at a BEB. We focus on what will happen if we set either $\hat{\mu} = \pm 1$ in (2.12). According to [7], classification of these simplest BEB transitions can be made as follows:

Persistence (or border-crossing). At the bifurcation point, an admissible equilibrium lying in the region S^+ becomes a boundary equilibrium and turns into a virtual equilibrium. Simultaneously, a virtual pseudoequilibrium becomes admissible. Thus, there is one admissible equilibrium on either side of the bifurcation, which is why this is termed persistence (see Figure 6(a)).

Nonsmooth fold. At the bifurcation point, the collision of two branches of admissible equilibria (one of which is pseudoequilibrium) is observed at the boundary equilibrium, before turning into two branches of virtual equilibria past the bifurcation point (see Figure 6(b)).

Theorem 2.5 (see [8]). *(Equilibrium transitions around a boundary equilibrium). For system* (2.1) *with* (2.8) *under* (2.11)*,*

1. persistence *is observed at BEB if* $\mathbf{C}\mathbf{A}^{-1}\mathbf{B} < 0$*;*
2. *a* nonsmooth fold *is observed if* $\mathbf{C}\mathbf{A}^{-1}\mathbf{B} > 0$.

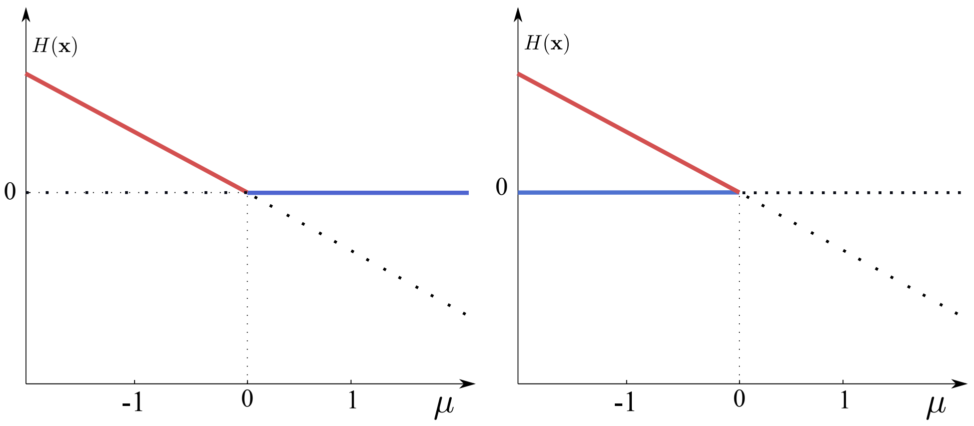

(a) persistence (b) fold

Figure 6. *Two typical BEB.* (a) *fold;* (b) *persistence.* (*admissible equilibria,* *pseudoequilibria, and* ⋯⋯ *virtual equilibria.)*

It is straightforward to find an explicit expression for the location and the stability of the pseudoequilibrium of the system (2.12) by direct calculation (2.14). Specifically, [8] argued that the stability of a pseudoequilibrium depends on the stability of the sticking set and the stability of the sliding vector field (2.5). Recalling the definition of the coefficient of restitution r and the condition that $0 < r < 1$ for the sticking set be stable, we find that the former can be guaranteed by

$$1 < \hat{\mathbf{C}}\hat{\mathbf{A}}\hat{\mathbf{B}} < 2 \quad \text{and} \quad a(\mathbf{y}) = \hat{\mathbf{C}}\hat{\mathbf{A}}^2\mathbf{y} < 0, \tag{2.15}$$

and the latter calculated from the eigenvalues of $\hat{\mathbf{A}}_s$ defined by (2.10). There is a 2-by-2 Jordan block corresponding to eigenvalue 0 with left eigenvector $\hat{\mathbf{C}}\hat{\mathbf{A}}$ and generalized eigenvector $\hat{\mathbf{C}}$. The other eigenvalues of $\hat{\mathbf{A}}_s$ determine the stability within the sliding flow and for stability should have negative real part.

Example 2.6. For a three-dimensional system defined by (2.12), we define the Jacobian $\hat{\mathbf{A}}$ in a generalized Liénard's form [6, 25] as

$$\hat{\mathbf{A}} = \begin{bmatrix} t & 1 & 0 \\ m & 0 & 1 \\ d & 0 & 0 \end{bmatrix},$$

and $\hat{\mathbf{C}}^\top = \mathbf{e}_1$, $\hat{\mathbf{B}} = [0, b_2, b_3]^\top$, $\hat{\mathbf{C}}\hat{\mathbf{A}}\hat{\mathbf{B}} = b_2, \hat{\mathbf{C}}\hat{\mathbf{A}}^{-1}\hat{\mathbf{B}} = \frac{b_3}{d}$. See the full derivation in Appendix B.

Further, the sticking set is explicitly derived as $\{\mathbf{y} \mid y_1 = 1, y_2 = -t, y_3 < -m\}$. To better understand the previous analysis framework and condition, two particular numerical cases are given:

1. When $[t, m, d, b_2, b_3]$ is selected as $[-0.7, -0.15, -0.025, 2.5, 0.625]$. The admissible equilibrium is stable, and persistence occurs according to Theorem 2.5. The location of pseudoequilibrium for $\hat{\mu} = +1$ is given as $\hat{\mathbf{y}}_0 = [1, 0.7, 0.05]^\top$ and the eigenvalues of $\hat{\mathbf{A}}_s$

are $0, 0, -0.25$, while $\hat{\mathbf{C}}\hat{\mathbf{A}}\hat{\mathbf{B}} > 2$, from which we conclude that the pseudoequilibrium is unstable.

2. When $[t, m, d, b_2, b_3]$ is selected as $[-0.7, -0.15, -0.025, 1.8, 1.6]$. The admissible equilibrium is stable, and persistence occurs according to Theorem 2.5. The location of the pseudoequilibrium for $\hat{\mu} = +1$ is given as $\hat{\mathbf{y}}_0 = [1, 0.7, 0.1219]^\top$ and the eigenvalues of $\hat{\mathbf{A}}_s$ re $0, 0, -0.8889$, while $\hat{\mathbf{C}}\hat{\mathbf{A}}\hat{\mathbf{B}} < 2$, from which we conclude that the pseudoequilibrium is stable. **AQ6**

Later, in section 4, we will show both of these two cases possess LCOs.

2.4. Bifurcation and stability of limit cycles. Under certain additional conditions, in addition to the transition from equilibria to pseudoequilibria, there can be a Hopf-like birth of an LCO at a BEB; see, e.g., [8, 11, 23, 24]. In accordance with the scale invariance of the normal form (2.12), the amplitudes of such limit cycles scale linearly with the bifurcation parameter and so can be studied just by setting $\hat{\mu} = \pm 1$ in the normal form. Specifically, in the two-dimensional case, equilibria and LCOs are the only possible attractors, there can be at most one limit cycle, and a stable limit cycle cannot coexist with a stable pseudoequilibrium. In higher dimensions, very little is known. In three dimensions, Carmona et al. [6] give the notion of invariant cones to add more information, but in general n dimensions the number of cases (at least $2n$ independent parameters [25]) that need to be considered seems to prohibit a general classification.

To consider the stability of limit cycles, one also has to be careful to construct the correct Poincaré map, because the pure monodromy matrix is not capable of giving us right conclusions. Instead, as introduced by Nordmark and collaborators (e.g., [10]), a correction called a *discontinuity mapping* is required whenever the trajectory interacts with a discontinuity boundary. The linearization of such mappings are known as a *Saltation matrix*; see [7] for a derivation. Specifically, for impacting systems with a single-impact boundary like (2.12), the saltation matrix for a point $\mathbf{y}^- \in \Sigma$ is given by

$$
\begin{aligned}
Q_y(\mathbf{y}^-) &= R_y(\mathbf{y}^-) + \frac{[F(R(\mathbf{y}^-)) - R_y(\mathbf{y}^-)F(\mathbf{y}^-)]\,H_y(\mathbf{y}^-)}{H_y(\mathbf{y}^-)F(\mathbf{y}^-)} \\
&= \mathbf{P} + \frac{[\mathbf{A} - \mathbf{P}\hat{\mathbf{A}}\mathbf{P}^{-1}]\hat{\mathbf{y}}\,\mathbf{C}}{\mathbf{C}\hat{\mathbf{A}}\mathbf{P}^{-1}\hat{\mathbf{y}}}.
\end{aligned} \tag{2.16}
$$

For a such system, Σ is a natural choice of the Poincaré section. Then we can construct a returning map as a composition of two parts ϕ_+ and ϕ_- to map Σ back to itself. Specifically, ϕ_+ is via evolution under flow (2.12) after some time $\tau(\mathbf{y})$ back to Σ, and $\phi_- = \mathbf{R}$ is the impact reset map in an impacting hybrid system. For a general orbit crossing the discontinuity manifold with $p \in \mathbb{Z}^+$ intersections, we can derive the full returning map as **AQ7**

$$
\Phi(\mathbf{y}) := (\phi_- \circ \phi_+)^p \cdot \mathbf{y}. \tag{2.17}
$$

3. Finding single-impact limit cycles. According to (2.17), a periodic orbit with p impacts per period, or simply a *period-p* orbit, with initial condition $\hat{\mathbf{y}} \in \Sigma$, should satisfy

$$
\Phi(\hat{\mathbf{y}}) = (\mathbf{R} \circ \phi_+)^p \cdot \hat{\mathbf{y}} = \hat{\mathbf{y}}. \tag{3.1}
$$

In this paper we consider only the case of $p=1$, for which

$$\left.\begin{aligned} \phi_+(\hat{\mathbf{y}}) &= \mathbf{y}^- \\ \mathbf{R}(\mathbf{y}^-) &= \hat{\mathbf{y}} \end{aligned}\right\} \to \mathbf{R}(\phi_+(\hat{\mathbf{y}}) = \hat{\mathbf{y}}. \tag{3.2}$$

In particular we require

$$H(\hat{\mathbf{y}}) = 0, \qquad \hat{v} := H_y F = \hat{\mathbf{C}}\hat{\mathbf{A}}\hat{\mathbf{y}} > 0. \tag{3.3}$$

According to (2.12), we can write $\phi^+ = \varphi(\hat{\mathbf{y}}, \hat{T})$, where $\varphi(\mathbf{y}, t)$ is the flow explicitly defined as $\mathrm{e}^{\hat{\mathbf{A}}\hat{T}}\hat{\mathbf{y}}$, and $\hat{T} = \tau(\hat{\mathbf{y}})$ is the *first* positive returning time, with initial condition $\hat{\mathbf{y}}$, given by

$$H(\varphi(\hat{\mathbf{y}}, \hat{T})) = \hat{\mathbf{C}}\mathrm{e}^{\hat{\mathbf{A}}\hat{T}}\hat{\mathbf{y}} - \hat{\mu} = 0. \tag{3.4}$$

Thus (3.2) can be explicitly expressed as

$$\mathbf{P}\mathrm{e}^{\hat{\mathbf{A}}\hat{T}}\hat{\mathbf{y}} = \hat{\mathbf{y}}. \tag{3.5}$$

Then (3.3) and (3.5) form a valid set of defining equations for a single-impact LCO of (2.12).

3.1. Formulation as a fixed-point problem.

Looking at (3.5), we see that the composed map (3.2) is effectively an eigenproblem. Finding the existence of an LCO can be simple if **AQ8** there is such a $\hat{\mathbf{y}}$ on a chosen Poincaré section that is an eigenvector of the matrix $\mathbf{P}\mathrm{e}^{\hat{\mathbf{A}}\hat{T}}$ corresponding to the unit eigenvalue, where the $\hat{T}$ is determined by the condition (3.4). Thinking of (3.5) as a shooting problem, we seek a state $\hat{\mathbf{y}}$ and a time $\hat{T} > 0$ to hit $H(\mathbf{y}) = 0$ again. All such $\hat{\mathbf{y}}$ must lie on an $n-2$ dimensional Euclidean subspace Ξ on the codimension-one surface on the switching set (2.13), which can be explicitly written as

$$\Xi := \{\hat{\mathbf{y}} \mid \hat{\mathbf{C}}\hat{\mathbf{y}} - \hat{\mu} = 0,\ \hat{\mathbf{C}}\mathrm{e}^{\hat{\mathbf{A}}\hat{T}}\hat{\mathbf{y}} - \hat{\mu} = 0\}. \tag{3.6}$$

Note that $\hat{T} \to \hat{\mathbf{y}} \in \Xi$ is a multivalued mapping, which is only locally invertible. Alternatively, we can view (3.5) as n equations in n unknown variables: $\hat{y}_i$, $i = 2, \ldots, n$ and $\hat{T}$.

Summarizing, we have the following.

Proposition 3.1. *For system* (2.12)*, if there exists* $\hat{\mathbf{y}}$ *given by* (3.3)*, and the induced* $\hat{T} > 0$ *by* (3.4) *such that* $\mathbf{P}e^{\hat{\mathbf{A}}\hat{T}}$ *has a unit eigenvalue, with corresponding eigenvector* $\hat{\mathbf{y}}$*, then an LCO must exist in this system with the period* $\hat{T}$*.*

Note that the proposition only provides a *nominal limit cycle;* in order to be a true limit cycle, we need an extra admissibility condition, that the trajectory should not contact Σ during $t \in (0, \hat{T})$. Such a condition is known as a *viability condition* [12].

Definition 3.2. *If the LCO determined by* $\hat{\mathbf{y}}$ *and* $\hat{T}$ *satisfies the following* viability condition*,*

$$H(\hat{\mathbf{C}}e^{\hat{\mathbf{A}}t}\hat{\mathbf{y}}) \geq 0 \quad \textit{for} \quad 0 < t < \hat{T},$$

we call it an admissible *LCO. Otherwise, it is termed a* virtual *LCO.*

Note that the viability condition is hard to check a priori but can easily be tested numerically once a nominal LCO has been found.

We now consider how to solve the shooting problem. Given the form of vector $\hat{\mathbf{C}} = \mathbf{e}_1^\top$ and (3.3), the initial condition $\hat{\mathbf{y}}$ should be

$$\hat{\mathbf{y}} = [\hat{\mu}, \hat{y}_2, \ldots, \hat{y}_n]^\top, \tag{3.7a}$$

which would give an n-dimensional search space. However, exploiting the eigenvalue problem, we note that the condition condition (3.5) can be reduced to finding a unit eigenvalue, which can be reduced to a a one-parameter line search for the scalar function

$$\boxed{p(\hat{T}) = \det(\mathbf{P}\mathrm{e}^{\hat{\mathbf{A}}\hat{T}} - \mathbf{I}) = 0.} \tag{3.7b}$$

Once we find such a $\hat{T}$, then $\hat{\mathbf{y}}$ can be easily reproduced as the nonzero eigenvector of $\lambda = 1$ satisfying (3.3), then the pair of $\hat{\mathbf{y}}$ and $\hat{T}$ represent initial conditions and period for a nominal LCO's initial condition, and all that is required is to check the viability condition through numerical evaluation of the matrix exponential in Definition 3.2 for all $t \in (0, \hat{T})$.

Corollary 3.3. *For system (2.12), if there exists $\hat{T} > 0$ such that (3.7b) is valid, and $\mathbf{P}e^{\hat{\mathbf{A}}\hat{T}}$'s corresponding eigenvector $\hat{\mathbf{y}}$ admits $\hat{\mathbf{C}}\hat{\mathbf{y}} \neq 0$, then the sign of the first component $\hat{\mathbf{y}}$ will be determined by (3.3), with specific $\hat{\mathbf{C}}\mathbf{A}\bar{\hat{y}} > 0$. We can then normalize this eigenvector so that the first coefficient is $\hat{\mu} = \pm 1$, which will determines the direction of bifurcation of LCO, and we call it*

1. *subcritical (surrounding an admissible equilibrium) LCO if $\hat{\mu} = -1$;*
2. *supercritical (surrounding a pseudoequilibrium) LCO if $\hat{\mu} = 1$.*

Proof. For an LCO with initial condition $\hat{\mathbf{y}}$ with corresponding period $\hat{T}$, from (3.7a), Figure 7, and Theorem 2.4's convention, we know

1. $\hat{\mu} = -1$ if $\mathbf{C}\hat{\mathbf{y}} = -1$, and $H(\mathbf{y}_0) = 1 > 0$ means the nominal equilibrium is an admissible equilibrium, which is surrounded by the found LCO;
2. $\hat{\mu} = 1$ if $\mathbf{C}\hat{\mathbf{y}} = 1$, and $H(\mathbf{y}_0) = -1 < 0$ means the nominal equilibrium is a virtual equilibrium, and only pseudotype equilibrium may exist, which is surrounded by the found LCO. ■

Combining the Corollary 3.3 and Definition 3.2, we now formulate a way to find meaningful (admissible) LCOs.

3.2. Stability of the LCO. LCOs satisfying (3.3) and (3.7) around BEB, as illustrated by Figure 7 and (3.2), are not guaranteed to be stable. Starting from a general case, to prove the stability of such an LCO, we need to find the Jacobian $\mathbf{J}$ around the fixed point $\hat{\mathbf{y}}$ using a chain rule,

$$\mathbf{J} = Q_y(\mathbf{y}^-)\, \phi_y^+(\hat{\mathbf{y}}, \hat{T}),$$

where the Q_y is the saltation matrix (2.16) and $\phi_y^+ = \mathrm{e}^{\hat{\mathbf{A}}\hat{T}}$.

Given the $\hat{T}$ and $\hat{\mathbf{y}}$, then $\mathbf{y}^-$ can be found via (B.3). Thus, we have can write the Jacobian derivative of the full hybrid system evaluated at the fixed point $\hat{\mathbf{y}}$ as

$$\mathbf{J}(\hat{\mathbf{y}}, \hat{T}) = \left(\mathbf{P} + \frac{[\hat{\mathbf{A}} - \mathbf{P}\hat{\mathbf{A}}\mathbf{P}^{-1}]\hat{\mathbf{y}}\,\mathbf{C}}{\mathbf{C}\hat{\mathbf{A}}\mathbf{P}^{-1}\hat{\mathbf{y}}} \right) \mathrm{e}^{\hat{\mathbf{A}}\hat{T}}. \tag{3.8}$$

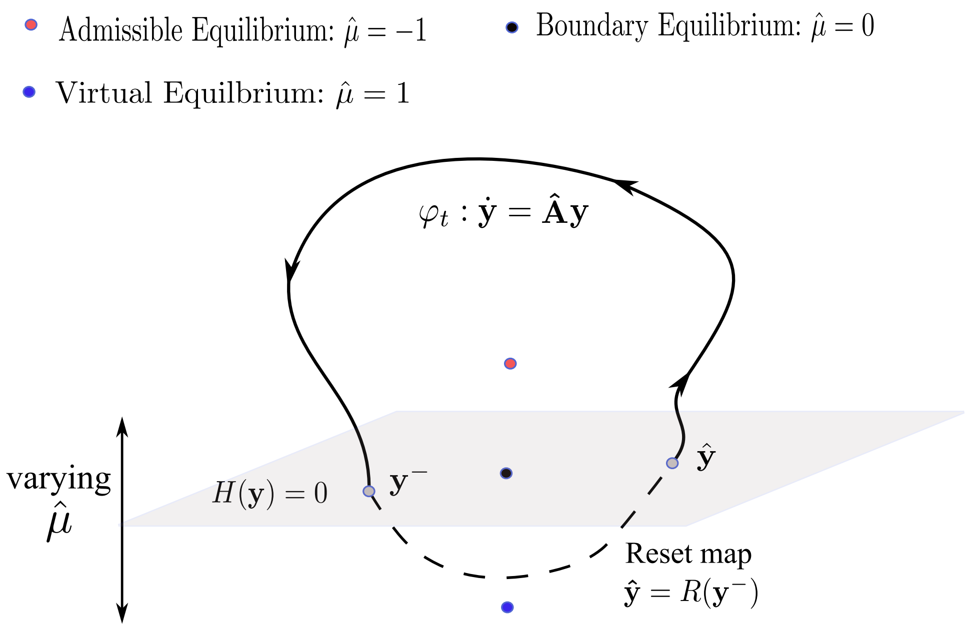

Figure 7. *Poincaré map of an LCO and the location of nominal equilibrium* $\mathbf{y}_0$*. Starting at* $\mathbf{y}^+$*, the trajectory arrives at the impacting surface again at* $\mathbf{y}^-$ *after evolution time* $\tau(\hat{\mathbf{y}})$*, and then via the zero-time reset map back to* $\mathbf{y}^+$ *to complete a periodic orbit.*

The following theorem regarding the stability of a periodic orbit can be found in noted dynamics books like [7, 17].

Theorem 3.4. *For an LCO, defined by* (3.3) *and* (3.7)*, of system* (2.12)*, the corresponding Floquet multipliers are given by the* n *eigenvalues of* $\mathbf{J}$ *defined by* (3.8)*, which are* $1, \lambda_2, \ldots, \lambda_n$*. If no Floquet multiplier* $\lambda_i (i = 2 \cdots n)$ *is outside the unit circle, the LCO is stable; otherwise it is unstable.*

3.3. Analytic formulae for three-dimensional examples. Now that we have conditions for the existence and stability of LCOs in the BEB normal form, it is instructive to try to seek explicit analytical formulae. We treat here the case $n = 3$. Using Theorem 2.4 and some further scaling of the matrices $\hat{A}$, $\hat{B}$, and $\hat{C}$, we can in principle derive a closed-form expression for $p(T)$ in (3.7b) in terms of a minimal number of parameters. Starting from unscaled matrices A, B, and C, there are two general nondegenerate cases, which can be distinguished by the eigenvalues of $\hat{\mathbf{A}}$:

Case I three real eigenvalues λ_1, λ_2, λ_3;

Case II a pair of conjugate complex eigenvalues $(-\alpha \pm \beta i)$ and a real one λ_3.

Without loss of generality, suppose that $\mathbf{A}$ is written in Jordan canonical form, and vectors $\mathbf{B}, \mathbf{C}$ are written in the corresponding basis. Specifically,

$$\mathbf{A} = \begin{bmatrix} \lambda_1 & 0 & 0 \\ 0 & \lambda_2 & 0 \\ 0 & 0 & \lambda_3 \end{bmatrix} \text{ for Case I, and } \mathbf{A} = \begin{bmatrix} \alpha & \beta & 0 \\ -\beta & \alpha & 0 \\ 0 & 0 & \lambda_3 \end{bmatrix} \text{ for Case II,} \tag{3.9}$$

and

$$\mathbf{C}^\top = \begin{bmatrix} \cos\theta\sin\varphi \\ \sin\theta\sin\varphi \\ \cos\varphi \end{bmatrix}. \tag{3.10}$$

Furthermore, we write

$$\mathbf{B} = b_2\mathbf{e}_\mathrm{k}^2 + b_3\mathbf{e}_\mathrm{k}^3$$

and define a transformation matrix

$$\mathbf{T} = [\mathbf{C}^\top, \mathbf{e}_\mathrm{k}^2, \mathbf{e}_\mathrm{k}^3], \tag{3.11}$$

where

$$\mathbf{e}_\mathrm{k}^2 = \begin{bmatrix} \cos\theta\cos\varphi \\ \sin\theta\cos\varphi \\ -\sin\varphi \end{bmatrix}, \ \mathbf{e}_\mathrm{k}^3 = \begin{bmatrix} -\sin\theta \\ \cos\theta \\ 0 \end{bmatrix}.$$

Then, we can derive explicit expressions for the matrices $\hat{\mathbf{A}}$, $\hat{\mathbf{A}}$, and $\hat{\mathbf{C}}$. The results are given in Appendix B. Under the assumption that $\lambda_3 \neq 0$, we can further reduce parameters by using $|\lambda_3|$ to rescale time, so that the set of values of λ_3 is reduced to two cases, $s = \pm 1$.

Thus, the parameter space Λ required to define all possible nondegenerate cases of a BEB for a general three-dimensional impacting hybrid system is

$$\{\lambda_1, \lambda_2, \lambda_3 = \pm 1, b_2, b_3, \theta, \varphi\},$$

which is seven-dimensional.

Remark 3.5. Another commonly chosen form of the Jacobian in the system (2.12) is the Liénard form [25], which is indeed covered by our general formulation. Note that Example 2.6 can be established with a special form of Jacobian along with $\varphi = \pi/2, \theta = 0$, which has two fewer parameters. For the general case, there is a simple transformation that can take the Jordan form definition into the Liénard form.

Thus, given the form (3.9) we can perform the necessary steps to compute the matrices $\hat{\mathbf{A}}$, $\hat{\mathbf{B}}$, and $\hat{\mathbf{C}}$. Then, by solving the linear differential equations explicitly, we can write down a closed-form expression for (3.7b) in terms of exponential and sinusoidal functions. The particular expressions for $p(T,\Lambda)$ are cumbersome; the respective formulae for Cases I and II are presented in (C.3) and (C.6) within Appendix B. Further, we can derive explicit expressions for $\hat{v}(\Lambda, T)$, the velocity of the initial condition of LCO, which determines the direction of bifurcation ($\hat{\mu} = +1$ or $\hat{\mu} = -1$); see (C.4) and (C.7). Moreover, given the explicit expression for any nominal LCO, we can check the viability condition, up to a solution of transcendental equations, and also determine the stability by computing the eigenvalues of (3.8).

Unfortunately, even restricting to three-dimensional cases we have to solve transcendental equations depending on seven parameters, and a complete classification of all possible cases seems to be a thankless task. Thus, we next seek numerical implementation of the conditions derived in this section.

4. Numerical examples. The conditions in Corollary 3.3 and Theorem 3.4 are not explicit. **AQ9** To analytically check their validity in a general n-dimensional system is tedious (see Appendix D and section 5 for some special cases). Therefore, we present a robust numerical algorithm. Suppose that $\hat{\mathbf{A}}, \hat{\mathbf{B}}, \hat{\mathbf{C}}$, etc., in canonical form of the system (2.12), are dependent on a set of parameters Λ. We also let $\boldsymbol{\Omega}$ be the principal submatrix of $(\mathbf{P}\mathrm{e}^{\hat{\mathbf{A}}T} - \mathbf{I})$ composed of all but the first row and column. Then we have

$$\mathbf{P}\mathrm{e}^{\hat{\mathbf{A}}T} - \mathbf{I} := \begin{bmatrix} \kappa & \mathbf{u}^\top \\ \mathbf{v} & \boldsymbol{\Omega} \end{bmatrix},$$

where $\mathbf{u}, \mathbf{v} \in \mathbb{R}^{(n-1)\times 1}$, and can write down the determinant monitoring function as

$$p(t;\Lambda) = \begin{cases} (\kappa - \mathbf{u}^\top \boldsymbol{\Omega}^{-1}\mathbf{v})\det(\boldsymbol{\Omega}) & \text{if} \quad \det(\boldsymbol{\Omega}) \neq 0, \\ \kappa \det(\boldsymbol{\Omega}) - \mathbf{u}^\top \operatorname{adj}(\boldsymbol{\Omega})\mathbf{v} & \text{for any} \det(\boldsymbol{\Omega}). \end{cases} \tag{4.1}$$

Once a root of $p(t) = 0$ is found, the candidate initial condition on Σ is given as

$$\hat{\mathbf{y}} = \hat{\mu}[1; -\boldsymbol{\Omega}^{-1}\mathbf{v}], \text{ provided } \det(\boldsymbol{\Omega}) \neq 0. \tag{4.2}$$

Finally Corollary 3.3 and Definition 3.2 are used to distinguish the type of LCO. The general algorithm is given in section 4, which we have implemented in MATLAB.

In the formulation of the algorithm, some details should be noticed:

1. Actually by substitution of (4.2) into (3.7), $\kappa - \mathbf{u}^\top \Omega^{-1}\mathbf{v} = 0$ is the first component of the equation, which is the returning condition (3.4).
2. When the Ω is close to singular at some time t_c, the value of $\hat{\mathbf{y}}$ will be stretched and **AQ10** this shows t_c is a potential lower/upper limit for $\hat{T}$, the period of a limit cycle.
3. Note that the roots of (3.7b) will not necessarily satisfy the viability condition, so a postprocessing set is required to integrate from the initial condition $\hat{\mathbf{y}}$ to check whether this is an admissible limit cycle or not.

We now provide some examples to show how the algorithm works in practice.

4.1. Planar examples. For a general planar system of the form (2.12), without loss of generality, we can write

$$\hat{\mathbf{A}} = \begin{bmatrix} 0 & 1 \\ b & a \end{bmatrix}, \mathbf{P} = \begin{bmatrix} 1 & 0 \\ 0 & -r \end{bmatrix}. \tag{4.3}$$

Then we have

$$\operatorname{trace}(\hat{\mathbf{A}}) = a, \quad \det(\hat{\mathbf{A}}) = -b, \quad \Delta = \operatorname{trace}^2(\hat{\mathbf{A}}) - 4\det(\hat{\mathbf{A}})$$

with

$$\mathbf{C}\hat{\mathbf{A}}^{-1}\mathbf{B} = [1, 0]\begin{bmatrix} -\frac{a}{b} & \frac{1}{b} \\ 1 & 0 \end{bmatrix}[0, (1+r)]^\top = \frac{1+r}{b}$$

and

$$\lambda_{1,2} = \frac{\operatorname{trace}(\hat{\mathbf{A}})}{2} \pm \frac{\sqrt{\Delta}}{2}.$$

Algorithm 4.1: LCO detection algorithm.

Data: Matrix $\mathbf{A}$, reset map matrix $\mathbf{P}$, searching region $[0,\ t_{\text{end}}]$, stepsize Δt, tolerance [tol].

Result: $\mathcal{N}$, the number of LCOs found; $\{\hat{\mathbf{y}}_{\text{i}}, T_{\text{i}}, \mathcal{M}_{\text{i}}, \mathcal{S}_{\text{i}}\},\ (i = 1, \dots, \mathcal{N})$ for each LCO, with initial condition $\hat{\mathbf{y}}_{\text{i}}$, corresponding period T_{i}, the corresponding biggest Floquet multiplier $\mathcal{M}_{\text{i}}$, and the value of $\hat{\mu}$ as $\mathcal{S}_{\text{i}}$.

/* Initialization */

$\tau \leftarrow 0, i \leftarrow 0$;

$\mathcal{N} \leftarrow 0,\ \hat{\mathbf{y}} \leftarrow [\,],\ \mathbf{T} \leftarrow [\,],\ \mathcal{M} \leftarrow [\,],\ \mathcal{S} \leftarrow [\,],\ P \leftarrow [\,],\ t \leftarrow [\,]$;

/* Begin search in given range */

$P[1] = 0, t[1] = 0$;

Function Det($\mathbf{A}$, $\mathbf{P}$, τ)**:**

- $\mathbf{K} \leftarrow \mathrm{e}^{\mathbf{A}\tau}$;
- $\Pi \leftarrow (\mathbf{PK} - \mathbf{I}), \quad \Omega \leftarrow \Pi(2:n, 2:n)$;
- $\kappa \leftarrow \Pi(1,1), \quad \mathbf{u}^\top \leftarrow \Pi(1, 2:n), \quad \mathbf{v} \leftarrow \Pi(2:n, 1)$;
- $p \leftarrow \kappa \det(\Omega) - \mathbf{u}^\top \operatorname{adj}(\Omega)\mathbf{v}$;
- **return** p, Ω, $\mathbf{v}$;

;

Function IC(Ω, $\mathbf{v}$, $\mathbf{A}$)**:**

- /* Compute the trial initial condition and sign of velocity */
- $\zeta \leftarrow -\Omega^{-1}\mathbf{v}, \quad \mathbf{y}_i \leftarrow [1; \zeta], \quad \hat{\mu} \leftarrow \operatorname{sign}(\mathbf{e}_\mathbf{1}^\top \mathbf{A}\mathbf{y}_i), \quad \mathbf{y}_i \leftarrow \hat{\mu}\mathbf{y}_i$;
- /* Find eigenvalue of J given by (3.8) with largest 2-norm */
- $\lambda \leftarrow \operatorname{eig}(J(\mathbf{y}_i)), \quad m \leftarrow \max(||\lambda_i||_2)$;
- **return** $\mathbf{y}_i$, $\hat{\mu}$, m;

;

Function store(τ, $\mathbf{T}$, $\mathbf{y}_i$, $\hat{\mathbf{y}}$, $\hat{\mu}$, $\mathcal{S}$, $\mathcal{N}$)**:**

- /* collect the solutions */
- **if** $\mathbf{C}\mathrm{e}^{\mathbf{A}\mathbf{t}}\mathbf{y}_i - \hat{\mu} \geq 0$ *for* $t \in (0, \tau)$ /* Check viability condition */ **then**
  - $\hat{\mathbf{y}} \leftarrow [\hat{\mathbf{y}}, \mathbf{y}_i]$;
  - $T \leftarrow [T, \tau], \quad \mathcal{M} \leftarrow [\mathcal{M}, m], \mathcal{S} \leftarrow [\mathcal{S}, s], \quad \mathcal{N} \leftarrow \mathcal{N} + 1$;
- **return** $\mathbf{T}$, $\hat{\mathbf{y}}$, $\mathcal{S}$, $\mathcal{N}$;

;

while $\tau \leq t_{\text{end}}$ **do**

- $\tau \leftarrow \tau + \Delta t$;
- $i \leftarrow i + 1$
- $p, \Omega, \mathbf{v} \leftarrow$ Det$(\mathbf{A}, \mathbf{P}, \tau)$;
- **if** $|p| < \text{tol}\ \&\ \det(\Omega) \neq 0$ **then**
  - $\mathbf{y}_i, s, m \leftarrow$ IC$(\Omega, \mathbf{v}, \mathbf{A})$;
  - $\mathbf{T}, \hat{\mathbf{y}}, \mathcal{S}, \mathcal{N} \leftarrow$ store$(\tau, \mathbf{T}, \mathbf{y}_i, \hat{\mathbf{y}}, \hat{\mu}, \mathcal{S}, \mathcal{N})$;
- **else if** $p \cdot P[i-1] < 0$ **then**
  - /* Interpolation to approximate */
  - $\tau \leftarrow \frac{pt[i-1] - \tau P[i-1]}{p - P[i]}$;
  - $p, \Omega, \mathbf{v} \leftarrow$ Det$(\mathbf{A}, \mathbf{P}, \tau)$;
  - $\mathbf{y}_i, s, m \leftarrow$ IC$(\Omega, \mathbf{v}, \mathbf{A})$;
  - $\mathbf{T}, \hat{\mathbf{y}}, \mathcal{S}, \mathcal{N} \leftarrow$ store$(\tau, \mathbf{T}, \mathbf{y}_i, \hat{\mathbf{y}}, \hat{\mu}, \mathcal{S}, \mathcal{N})$;
- $t[i] = \tau$;
- $P[i] = p$;

Table 1

Illustration of the results for the cases of planar BEB in the persistence and focus-focus transition case with $\Delta < 0$. *(*AE*: **A**dmissible **E**quilibrium; PE: **P**seudo **E**quilibrium; U: **U**nstable; S: **S**table; null: not given. For conditions in* [8], trace($\mathbf{A}$) < 0 *indicates stable equilibrium and* $re^{\frac{\alpha}{\omega}\pi} < 1$ *implies stable LCO, and vice versa.)*

	Case	1	2	3	4
	{a,b,r}	$-1,\,-1,\,1.5$	$-1,-1,7.0$	$0.5,-1,0.5$	$0.5,-1,0.4$
	Graph	*Figure* 9	*Figure* 10	*Figure* 11	*Figure* 12
Classification by results in [8]	trace($\mathbf{A}$)	<0	<0	>0	>0
	$re^{\frac{\alpha}{\omega}\pi}$	0.2446	1.1412	1.1235	0.9002
	AE	**S**	**S**	**U**	**U**
	PE	null	null	null	null
	LCO type	**S**	**U**	**U**	**S**
Classification by Algorithm 4.1	AE	**S**	**S**	**U**	**U**
	PE	**U**	**U**	**S**	**S**
	$\mathcal{N}$	1	1	1	1
	$\mathcal{M}$	$=1$	>1	>1	$=1$
	$\hat{\mu}$	1	-1	1	-1
	LCO type	**SSuper**	**USub**	**USuper**	**SSub**

Then, according to Theorem 2.5 and the further results in [8], we have

1. $b > 0$ leads to a nonsmooth fold for which the admissible equilibrium is a saddle, with one positive and one negative eigenvalue;
2. $b < 0$ corresponds to persistence with two subcases depending on the sign of Δ:
   (a) $\Delta > 0$ implies the admissible equilibrium is a node, being stable when trace($\hat{\mathbf{A}}$) < 0 and unstable when trace($\hat{\mathbf{A}}$) > 0;
   (b) $\Delta < 0$ implies the admissible equilibrium is focus, being stable when trace($\hat{\mathbf{A}}$) < 0 **AQ11** and unstable with trace($\hat{\mathbf{A}}$) > 0.

Let us consider item 2(b). The results of applying Algorithm 4.1 and the theorems in [8] are summarized in Table 1, and the resulting phase portraits are illustrated in Figures 9 to 12, in which the results show good agreement between the two methods. Note, however, that the case shown in Figure 12, for which there is the subcritical existence of a stable LCO, is not treated explicitly in [8].

We next present a particular two-dimensional example that illustrates the importance of the viability condition.

Example 4.1. Let us pick a specific example of the form (4.3), when we set

$$a = -0.2;\ b = -1.01; r = 3.0796.$$

The results are shown in Figure 8 and some virtual LCOs are found by the algorithm.

4.2. Three-dimensional examples. First, let us revisit Example 2.6, for which there is a transition from a stable focus for $\hat{\mu} = -1$. The first subcase has an unstable pseudoequilibrium, and the other case possesses a stable one for $\hat{\mu} = +1$. Apart from the transition of equilibria, whether any LCO is born was previously unknown.

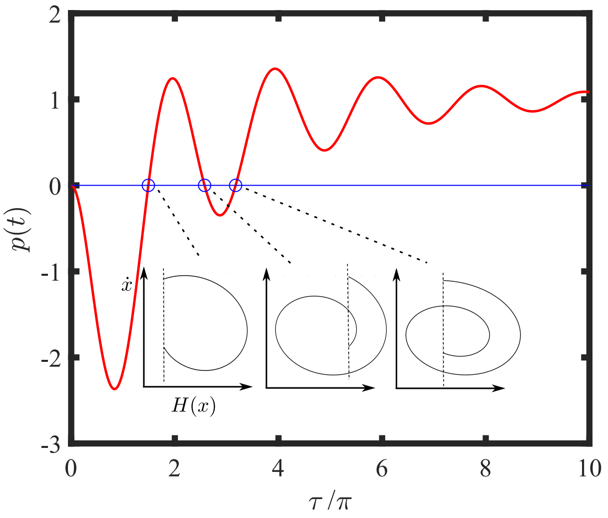

Figure 8. *The function $p(t)$ for Example 4.1. Note that the first root leads to an admissible LCO whereas the next two are virtual.*

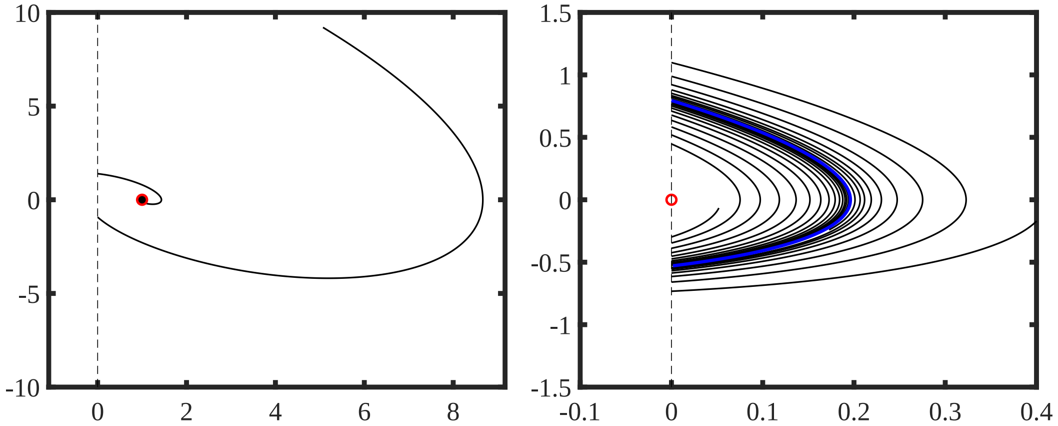

(a) $\mu = -1$ (b) $\mu = 1$

Figure 9. *Illustration of the phase portrait before and after bifurcation for Case 1 in Table 1 (▬ represents stable LCO; - - - represents unstable LCO; ● stands for stable equilibrium; ∘ stands for unstable equilibrium; - - - - is the switching surface.)*

Example 4.2. (Example 2.6 continued.) To look for possible LCOs, we can turn to the condition (3.7b) and Algorithm 4.1. Table 2 gives us the answer: both subcases possess supercritical LCOs. Specifically, we find the coexistence of a stable pseudoequilibrium and a stable LCO, which also happened in the motivating example in subsection 1.1. Such a phenomenon is impossible in a planar system, but clearly can be found in three dimensions.

While a complete classification in three dimensions seems complex, we can use the analytic calculations in subsection 3.3 to find certain degenerate cases, variation across which causes a change in the criticality of the bifurcation.

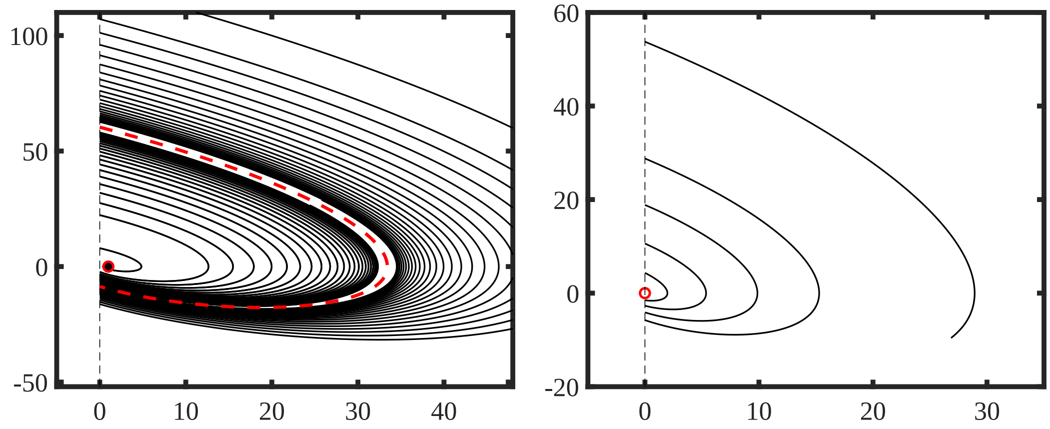

(a) $\mu = -1$ (b) $\mu = 1$

Figure 10. *Similar to Figure 9, but for Case 2 in Table 1.*

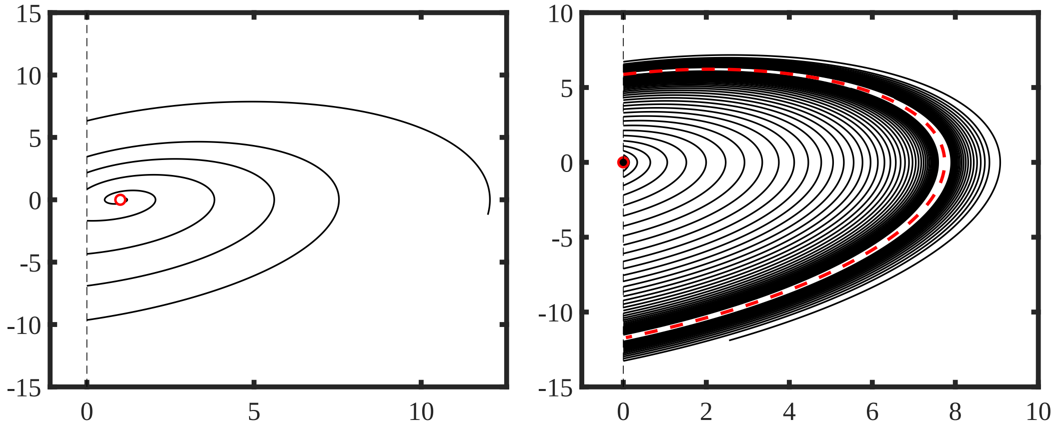

(a) $\mu = -1$ (b) $\mu = 1$

Figure 11. *Similar to Figure 9, but for Case 3 in Table 1.*

For example, from the general expressions in (C.4) and (C.7), the velocity $\mathbf{v}$ will be zero when $\lambda_{1,2,3} = 0$ for Case I and $\lambda_3 = 0$ for Case II. These conditions lead to a singular Jacobian, which gives conditions for changes of criticality. If v and $p(t)$ are both smoothly defined around $\lambda_i = 0$ and $\frac{\partial v}{\partial \lambda_i} \neq 0$, then according to the implicit function theorem, the sign change of λ_i around 0 will change the sign of v. Following Algorithm 4.1, the change of velocity sign indicates the change of the LCO type by Corollary 3.3, thus switching the BEB bifurcation between supercritical and subcritical.

Example 4.3. (Switch of bifurcation type). For Case I, we design two models which differ only in the sign of λ_2, and for Case II, we design two models which differ only in the sign of λ_3. Specific parameter values are

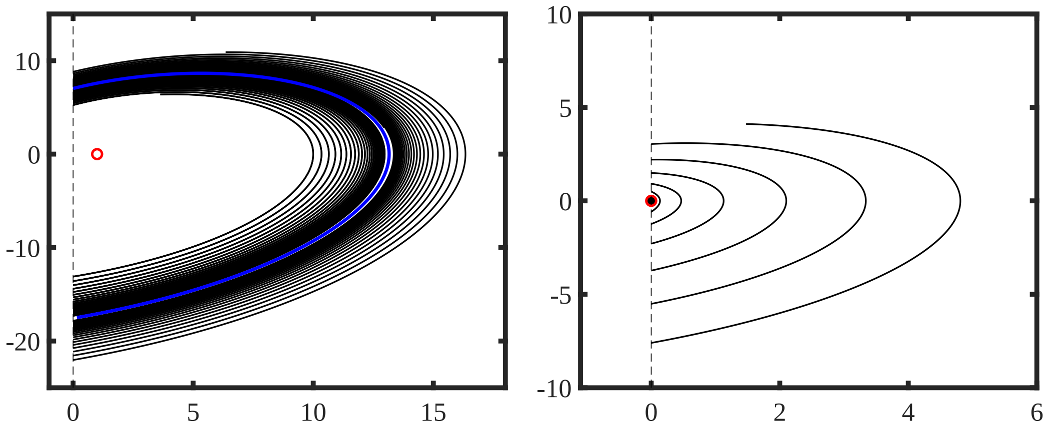

(a) $\mu = -1$ (b) $\mu = 1$

Figure 12. *Similar to Figure 9, but for Case 4 in Table 1.*

Table 2

*Further analysis of the two three-dimensional cases with persistence in Example 2.6, where LCOs emerge due to focus transition (from Algorithm 4.1). The parameter $[t, m, d]$ is selected as $[-0.7, -0.15, -0.025]$. (AE: **A**dmissible **E**quilibrium; PE: **P**seudo **E**quilibrium; U: **U**nstable; S: **S**table.)*

Graph	b_2, b_3	**AE**	**PE**	$\mathcal{N}$	$\mathcal{M}$	$\hat{\mu}$
Figure 13a and Figure 13b	$b_2 = 2.5$, $b_3 = 0.625$	**S**	**U**	1	$= 1$	1
Figure 13c and Figure 13d	$b_2 = 1.8$, $b_3 = 1.600$	**S**	**S**	2	> 1, $=1$	1

Table 3

*Two subcases with persistence and LCO type change (from Algorithm 4.1). (AE: **A**dmissible **E**quilibrium; PE: **P**seudo **E**quilibrium; U: **U**stable; S: **S**table.)*

	parameters $\hat{\Lambda}$	AE	PE	$\mathcal{N}$	$\mathcal{M}$	$\hat{\mu}$	Diagram	p(t)
Case I	(i)	US	US	1	$= 1$	-1	*Figure 14a*	Figure 15b
	(ii)	S	US	1	$= 1$	1	*Figure 14b*	
Case II	(i)	US	US	1	$= 1$	-1	*Figure 14a*	Figure 15c
	(ii)	S	US	1	$= 1$	1	*Figure 14b*	

Case I: $\lambda_1 = -1$, $\lambda_3 = -1$, $b_2 = 129.3652$, $b_3 = 15.4041$, $\phi = 0.8761$, $\theta = 0.0083$;
and (i): $\lambda_2 = 0.01$, (ii): $\lambda_2 = -0.01$;
Case II: $\lambda_1 = -10 + 10\mathrm{i}$, $\lambda_2 = -10 - 10\mathrm{i}$, $\lambda_3 = 1$, $b_2 = 0.2332$, $b_3 = 0.2251$, $\phi = 1.5002$, $\theta = 2.3562$;
and (i): $\lambda_3 = 1$, (ii) $\lambda_3 = -1$.

The results are summarized in Table 3 and depicted in Figure 14. In both cases, the switch of bifurcation from subcritical to supercritical can be clearly seen. The corresponding graphs of $p(t)$ are shown in Figure 15(a).

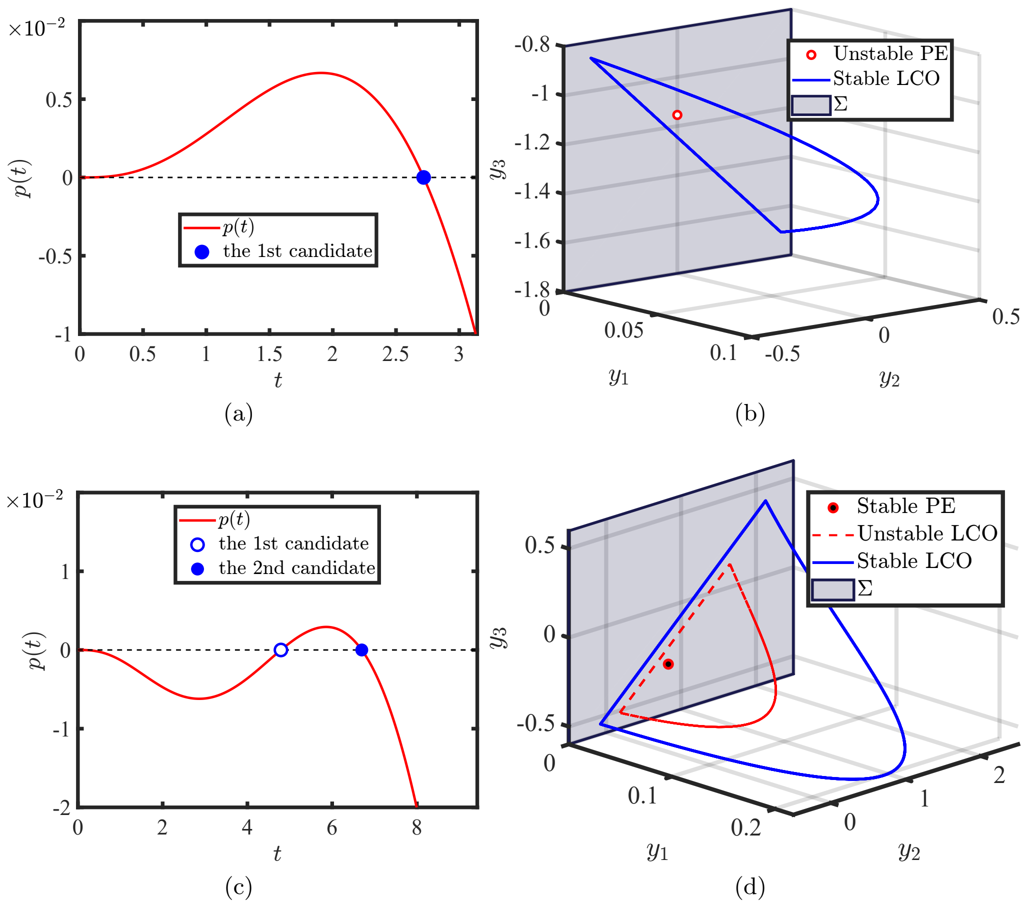

Figure 13. *LCOs in Example 2.6 using Algorithm 4.1. We find for $\hat{\mu} = 1$, subcase 1 in the first row of Table 2*—(a), (b): *a stable LCO exists, surrounding an unstable pseudoequilibrium; subcase 2 in the second row of Table 2*—(c), (d): *two LCOs with different stability exist surrounding a stable pseudoequilibrium.*

4.3. Airfoil model in $\mathbb{R}^8$. We now return to the motivating example from the beginning of the paper, the airfoil model. Set $\bar{U} = 0.64833$ in (1.1) and we use Algorithm 4.1 to explain the BEB result computed by brute force. The results of applying Algorithm 4.1 are depicted in Figure 16. This reveals that actually two LCOs bifurcate, the one observed in Figure 2(b) and Figure 3 and a another smaller-amplitude one. As part of the algorithm, we compute the largest Floquet multipliers using (3.8) to determine stability, which shows the smaller limit cycle has a multiplier outside the unit circle, which confirms its instability whereas the larger-amplitude LCO is stable. A comparison is made between the stable LCO found in direct numerical simulation and the one found by our method as shown in Figure 17.

5. Discussion. We already showed in subsection 3.3 that even for three-dimensional examples, a complete classification of bifurcation outcomes from a BEB is problematic, owing to the curse of dimensionality and the lack of a center-manifold-like result for impacting hybrid systems. Thus, a complete unfolding of BEBs for n-dimensional cases is clearly not feasible. Instead, in this section we focus on a few additional analytical considerations that are in the

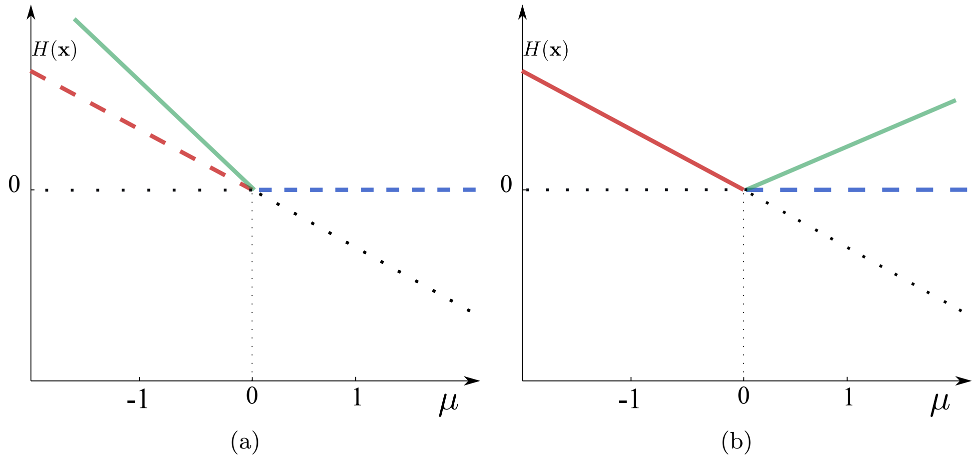

Figure 14. *Qualitative representation of LCO emerges via* (a) *subcritical;* (b) *supercritical bifurcation.* *stable admissible equilibrium;* *unstable admissible equilibrium;* *stable pseudoequilibrium;* *unstable pseudoequilibrium;* *stable LCO;* ····· *virtual equilibrium.*

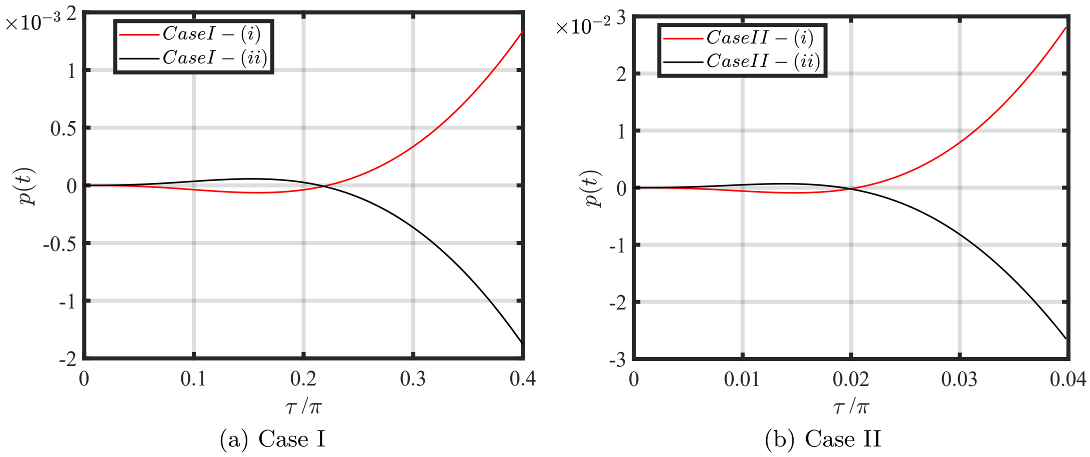

Figure 15. $p(t)$ *of the cases in Table* 3*.*

direction of establishing more general conditions for the bifurcation of LCOs at a BEB, with more precise details left for future work.

First, we illustrate in subsection 5.1 how Algorithm 4.1 is well suited for numerical continuation. Then, in subsection 5.2 we return to three dimensions and attempt to gain geometrical insight into what conditions can lead to the coexistence of a stable limit cycle and a stable pseudoequilibrium. Finally, in subsection 5.3 we we look at the behavior of $p(t)$ as an analytic function of t and attempt to establish a sufficient condition for the bifurcation of LCO. Finally, we draw conclusions in subsection 5.4.

5.1. Numerical continuation. The condition (3.7b) leads to a smoothly defined scalar function $p(\Lambda, t)$, albeit one that can develop isolated singularities. Hence, it is well set up for

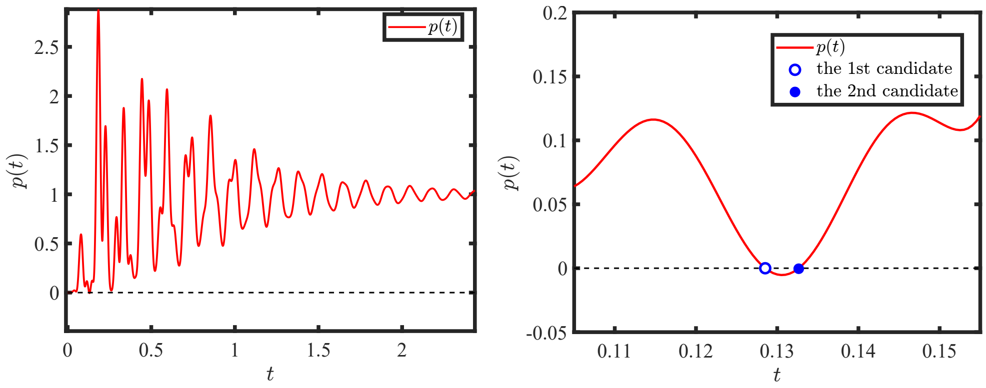

(a) (b)

Figure 16. (a) *LCO searching for the airfoil example* (1.1) *by Algorithm* 4.1*. Two LCOs with opposite stability are found after the BEB when* $\hat{\mu}=1$*.* (b) *Zoomed-in close to the first two zeros of* $p(t)$*.*

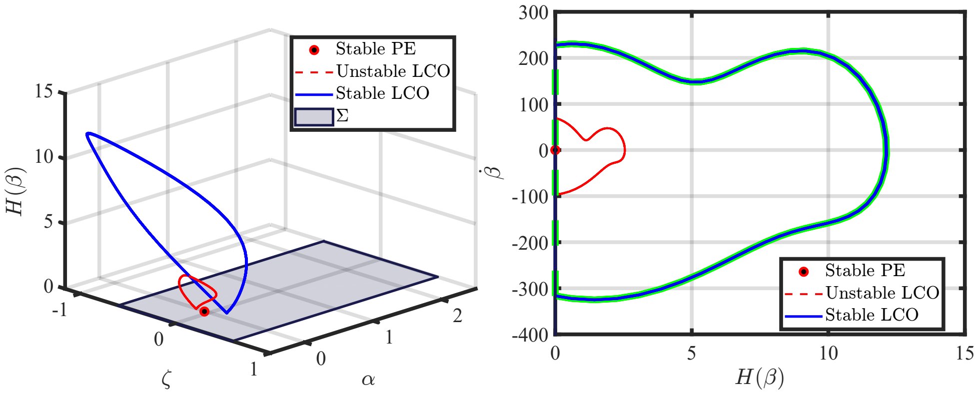

(a) Illustration for the $p(t)$ (b) Zoomed-in region with roots

Figure 17. $[\Delta\bar{U}=1\times10^{-3}]$. *Phase portrait of the two LCOs for wing-flap example* (1.1) (a) *phase portrait of* $\zeta,\alpha,H(\beta)$*, where* $H(\beta)$ *measure the state* β*'s distance to the impacting surface (see Definition* 2.1 *and Theorem* 2.4*);* (b) *phase portrait of flap degree* β*, with* ▪▪▪ *for the LCO A in Figure* 3(a) *scaled by* 1.41×10^5 *according to scaling* (B.2) *in Theorem* 2.4*, and* ▬ *stands for the stable LCO found by our algorithm. The good match shows they are the same LCO of the wing flap system.*

numerical continuation [1, 22]. Thus, we can easily extend Algorithm 4.1 in order to track solutions in parameter space. We have extended our MATLAB implementation by coding up a bespoke version of pseudoarclength continuation. We illustrate the method by applying it to the wing-flap model (1.1). We choose the coefficient of restitution r and damping ratio ξ as our two bifurcation parameters, as both are known to play a crucial role within mechanically vibrating systems. Figure 18(a) shows the results for the bifurcation diagram of period T^* against r. Here we see that the two limit cycles merge and disappear in a (smooth) cyclic fold for $r_{\mathrm{cr}}\approx 0.6292$. This gives rise to the birth of two limit cycles of opposite stability, explaining our earlier numerical results for $r=0.72$ in Figure 17. Figure 18(b) shows the result of a variation of ξ; we note that values of the damping coefficient that are either two high or too **AQ12**

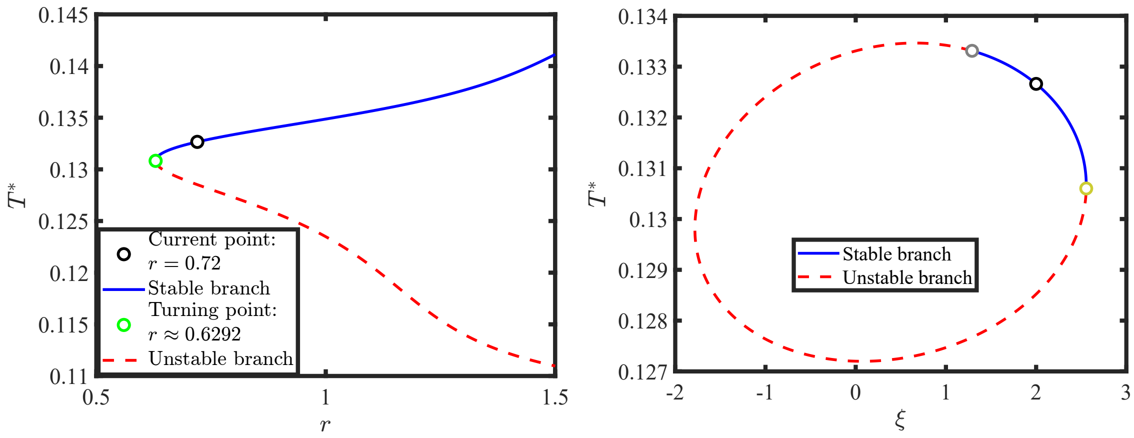

(a) Varying restitution coefficient (b) Varying structural damping

Figure 18. *Parametric analysis via numerical continuation.* (a) ○ *current point with* $r = 0.72$; ○ *the folding point* $r = 0.6292$; (b) ○ *critical point* $\xi = 1.29\%$, *where one Floquet multiplier crosses the unit circle via negative half axis;* ○ *current point with* $\xi = 2\%$; ○ $\xi = 2.556\%$.

low will destroy the LCOs. For example, there is no stable LCO when the damping ratio is below a critical value $\xi \approx 1.29\%$.

5.2. Geometrical interpretation of the reset map in three dimensions. From the point of view of an impacting mechanical system, it is interesting to ponder how a stable limit cycle can coexist with a stable pseudoequilibrium for $0 < r < 1$. This behavior we observed in the motivating wing-flap example seems counterintuitive. Intuitively, we would need a mechanism to add additional energy to the system from the amount of energy required to sustain the stable pseudoequilibrium. Yet if $0 < r < 1$, each impact removes energy (at least from the degree of freedom normal to the rigid surface). The resolution of this apparent paradox comes about due to the reset map transferring energy into directions other than that normal to Σ. It would seem in (1.1) that it is the nonconservative aerodynamic forces that enable this energy transfer to happen. But that model has an eight-dimensional phase space, so for ease of understanding we consider the situation for three-dimensional models, for which in subsection 3.3 we have complete analytic information.

Note from (2.12) the reset map is affine to leading order. In three dimensions, the grazing set Σ^0 is a line $\ell := \{\mathbf{y} \mid H(\mathbf{y}) = 0, \mathbf{CAy} = 0\}$, which we depict Figure 19. Then the reset map defines a degree of stretch in both the lateral and perpendicular directions, namely,

$$R \circ \begin{bmatrix} 0 \\ y_1^- \\ y_3^- \end{bmatrix} = \begin{bmatrix} 0 \\ y_2^- \\ y_3^- \end{bmatrix} + z^+(\rho^-, z^-)\mathbf{e}_z + \rho^+(\rho^-, z^-)\mathbf{e}_\rho,$$

and here $\mathbf{e}_\rho = [0, \frac{a_{12}}{\sqrt{a_{12}^2+a_{13}^2}}, \frac{a_{13}}{\sqrt{a_{12}^2+a_{13}^2}}]^\top$ and $\mathbf{e}_z = [0, \frac{a_{13}}{\sqrt{a_{12}^2+a_{13}^2}}, \frac{-a_{12}}{\sqrt{a_{12}^2+a_{13}^2}}]^\top$ are the unit directional vector along and orthogonal to ℓ, respectively. Specifically, we have $\rho = \frac{1}{\sqrt{a_{12}^2+a_{13}^2}}\mathbf{CAy} = \frac{1}{\sqrt{a_{12}^2+a_{13}^2}} v$.

Bearing in mind the definition (2.4), we can write $\rho^+ = -(1+r)\rho^-$, where $r(\rho^-, z^-) > 0$ is the effective restitution coefficient. Furthermore, let us write $z^+ = R_z(\rho^-, z^-)\rho^-$. For a

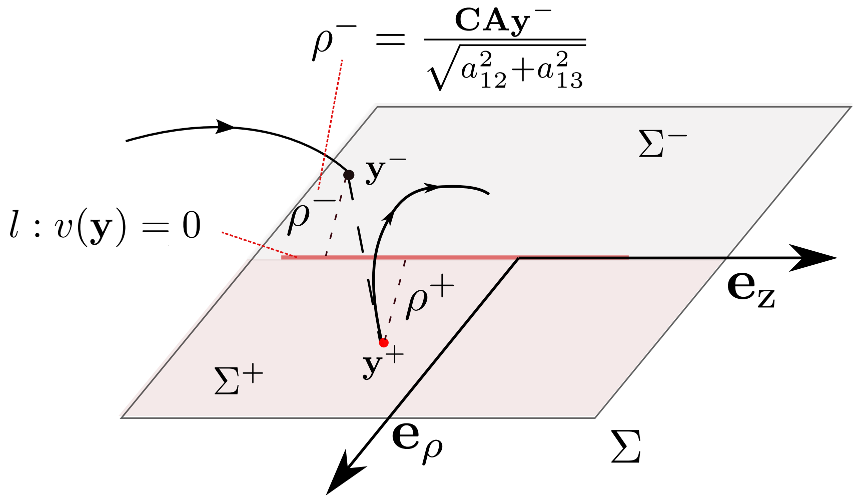

Figure 19. *A geometric sketch of the reset map.*

given set of parameters in (C.2) and (C.5), the stretching coefficients r and R_z can be written explicitly. Specifically, for the focus case we get

$$\begin{aligned}\begin{bmatrix} r \\ R_z \end{bmatrix} &= -\begin{bmatrix} a_{12} & a_{13} \\ -a_{13} & a_{12} \end{bmatrix}\begin{bmatrix} b_2 \\ b_3 \end{bmatrix} - \begin{bmatrix} 1 \\ 0 \end{bmatrix} \\ &= -\begin{bmatrix} (\alpha-\lambda_3)\sin\varphi\cos\varphi & \beta\sin\varphi \\ -\beta\sin\varphi & (\alpha-\lambda_3)\sin\varphi\cos\varphi \end{bmatrix}\begin{bmatrix} b_2 \\ b_3 \end{bmatrix} - \begin{bmatrix} 1 \\ 0 \end{bmatrix}.\end{aligned} \tag{5.1}$$

Now, let us consider two cases with the same Jacobian $\mathbf{A}$ but with different reset maps. Specifically, the two cases in Example 4.2 having different reset maps. Note that in this example, the eigenvalues of $\mathbf{A}$ all have strictly negative real parts. Thus, for $\mu = -1$ there is an asymptotically stable equilibrium. For the two cases in Table 2 we can compute

$$1. \quad r = 1.5, \quad R_z = 0; \qquad 2. \quad r = 0.8, \quad R_z = 4.6.$$

We saw how both cases led to supercritical bifurcation of an LCO, but with different kinds of bifurcation. In the first case, the coefficient of restitution $r > 1$, which explains how additional energy enters through impact. Indeed, in this case, the pseudoequilibrium is unstable. In the second case, while the effective coefficient of restitution $r < 1$, there is a large component of the rest map in the $\mathbf{e}_z$ direction. It is this coupling of velocity (perpendicular to ℓ) into the displacement in the direction transverse to ℓ that enables a stable limit cycle to emerge. In effect, energy is being gained by the z-component, which is compensated for during the free **AQ13** motion. Such a limit cycle can coexist with a stable pseudoequilibrium, whose stability mostly comes about because of the stability of the sticking set, which is ensured because $0 < r < 1$.

5.3. Toward a sufficient condition for a limit cycle. An alternative way to think about the mechanism for the generation of limit cycles in n-dimensional BEBs is to consider an analytic form for $p(t)$, using the matrix exponential. As in the previous example, we shall consider the simplified case that $\mathbf{A}$ is asymptotically stable (sometimes called a Hurwitz matrix), that is, all its eigenvalues are in the left-half complex plane.

Consider the form of $p(t)$ given by (3.7b). Recall that $\mathbf{P} = \mathbf{I} - \hat{\mathbf{B}}\hat{\mathbf{C}}\hat{\mathbf{A}}$, and hence it is straightforward to show that $\mathbf{P}$ has eigenvalues equal to 1, with multiplicity $n-1$, and $-r$ with multiplicity 1. Moreover, because $\mathbf{A}$ is Hurwitz, the eigenvalues of $\mathbf{P}e^{\mathbf{A}T} - \mathbf{I}$ will each approach -1. Hence

$$\lim_{t\to\infty} p(t) = \lim_{t\to\infty} \det(\mathbf{P}e^{\mathbf{A}t} - \mathbf{I}) = (-1)^n. \tag{5.2}$$

Meanwhile, we notice that $p(0) = 0$, so an important piece of information is to work out the sign of $p(t)$ for small t. The details are given in Appendix D. There we find that

$$p(t) = -\frac{1}{2}(r-1)\det(\mathbf{A})t^n + \mathcal{O}(t^{n+1}). \tag{5.3}$$

Combining (5.2) and (5.3) we can state our first result with $\mathrm{sign}(\mathbf{A}) = (-1)^n$, namely,

$$\text{if } r > 1, \text{ then } \mathrm{sign}\left(\lim_{t\to 0^+} p(t)\right) \neq \mathrm{sign}\left(\lim_{t\to\infty} p(t)\right). \tag{5.4}$$

It is thus tempting to appeal to the intermediate value theorem to show that there must therefore be a zero of $p(t)$ for some finite value $t = \hat{T}$. Unfortunately, there are two caveats: first, one would need to check the viability condition, and, second, there is no guarantee that $p(t)$ does not develop a singularity. In principle, these caveats can be dealt with by writing down explicit conditions on the matrix exponential. But the details are left to future work.

Incidentally, the converse of (5.4) also applies:

$$\text{if } 0 < r < 1, \text{ then } \mathrm{sign}\left(\lim_{t\to 0} p(t)\right) = \mathrm{sign} \lim_{t\to\infty} p(t)).$$

This condition goes some way to explaining why the stable limit cycle we found that coexists with the stable pseudoequilibrium for $0 < r < 1$ has to be coexisting with another (albeit unstable) limit cycle. If the function $p(t)$ avoids any singularities as t increases from zero, then we would have to have an even number of zero crossings, which would correspond to an even number of nominal LCOs.

5.4. Conclusion. In summary, in this paper, we have attempted to shed more light on the analysis of Hopf-like bifurcation of limit cycles at boundary equilibrium bifurcations in piecewise-smooth systems. Specifically, we have dealt with the case of impacting hybrid systems. In fact, in [8], it is shown how BEB normal form analysis for impacting hybrid systems can be regarded as a special case of *piecewise-smooth continuous* and *Filippov* systems, at least when one considers only equilibria and pseudoequilibria. In principle, the approach adopted here for finding LCOs could be extended to deal with piecewise-smooth continuous systems. However, now $p(t)$ would become a function of two parameters $p(t_1, t_2)$, where t_1 and t_2 are the a priori unknown times spent under the regular flow and the sliding flow. An investigation of this will form the subject of future work.

Another weakness of the present work is that we look only at limit cycles. For systems with sufficiently high dimensionality, other attractors such as invariant tori or chaotic attractors may also occur locally at a BEB. For example, numerical evidence for a particular three-dimensional system in [13] suggests local birth of chaotic attractors at a BEB in an impacting hybrid system. A full unfolding of that case is pending.

Even within the realm of LCOs at BEBs of impacting hybrid systems, there remain many analytical details that we have not fully explored in this paper. The arguments presented in this section suggest that, provided we can get a control of possible singularities of $p(t)$, then it may be possible to derive sufficient conditions for N limit cycles to bifurcate, owing to sign changes of $p(t)$. We have also avoided any discussion of degenerate cases, for which one has to go beyond the scale-invariant normal form.

Appendix A. Full equations of motion for airfoil model. The model studied in subsection 1.1 is a reduced-order model of a two-dimensional airfoil within a constant air stream. A full derivation can be found in [27]; here we just present enough information to specify the equations in full. The three mechanical degrees of freedom are α, β, and ζ. The first two represent the angular displacement (pitch) of the airfoil and flap, respectively; and $\zeta = h/b$ is the dimensionless displacement in the heave degree of freedom, normalized by semichord b. The parameter $\bar{U} = U/\omega_\alpha b$ is a dimensionless measure of the magnitude of the free stream air velocity approaching the airfoil, and the parameter δ characterizes the amount of flap freeplay.

Using Lagrangian mechanics, it is straightforward to write down the equations of motion of the mechanical degrees of freedom in the form

$$\overline{\boldsymbol{M}}\begin{bmatrix}\ddot{\zeta}\\ \ddot{\alpha}\\ \ddot{\beta}\end{bmatrix} + \overline{\boldsymbol{C}}\begin{bmatrix}\dot{\zeta}\\ \dot{\alpha}\\ \dot{\beta}\end{bmatrix} + \overline{\boldsymbol{K}}\begin{bmatrix}\zeta\\ \alpha\\ \beta\end{bmatrix} = \begin{bmatrix}L/(mb)\\ T_\alpha/mb^2\\ T_\beta/(mb^2)\end{bmatrix} + \left[\mathbf{F}\right], \tag{A.1}$$

$$\text{where} \quad \overline{\boldsymbol{M}} = \begin{bmatrix}1 & \bar{x}_\alpha & \bar{x}_\beta\\ \bar{x}_\alpha & \bar{r}_\alpha^2 & \bar{r}_\beta^2 + \bar{x}_\beta(\bar{c}-\bar{a})\\ \bar{x}_\beta & \bar{r}_\beta^2 + \bar{x}_\beta(\bar{c}-\bar{a}) & \bar{r}_\beta^2\end{bmatrix},$$

$$\overline{\boldsymbol{K}} = \begin{bmatrix}\omega_h^2 & 0 & 0\\ 0 & \omega_\alpha^2\bar{r}_\alpha^2 & 0\\ 0 & 0 & \omega_\beta^2\bar{r}_\beta^2\end{bmatrix} \text{ and } \overline{\boldsymbol{C}} = (\Phi^T)^{-1}\begin{bmatrix}2\xi_h\omega_h & 0 & 0\\ 0 & 2\xi_\alpha\omega_\alpha\bar{r}_\alpha^2 & 0\\ 0 & 0 & 2\xi_\beta\omega_\beta\bar{r}_\beta^2\end{bmatrix}\Phi^{-1},$$

where Φ is an eigenvector matrix defined by $(\overline{\boldsymbol{K}} - \omega^2\overline{\boldsymbol{M}})\phi_i = 0$, $\Phi = [\phi_1 \dots \phi_n]$, and $\Phi^T\overline{\boldsymbol{M}}\Phi = \boldsymbol{I}$. Also, L, T_α, and T_β define state-dependent generalized aerodynamic forces, defined below, and $\mathbf{F}$ represents other external generalized forces (set to zero in the current model, except for preload $1\% \cdot \delta k_\beta$ in the component corresponding rotational flag degree). The ξ_i, for $i \in \{h, \alpha, \beta\}$, corresponds to mode-proportional structural damping ratios for each degree of **AQ16** freedom; by default we set the reasonable value $\xi_i = \xi = 0.02$ for each degree of freedom (cf. [29]).

The unsteady aerodynamics L, T_α, T_β are given as

$$\begin{aligned}
\text{(A.2a)} \qquad L &= \pi\rho_a b^2 \left(\ddot{h} + V\dot{\alpha} - b\bar{a}\ddot{\alpha} - \frac{V}{\pi}T_4\dot{\beta} - \frac{b}{\pi}T_1\ddot{\beta}\right) \\
&\quad + 2\pi\rho_a V b \left(Q_a(\hat{\tau})\phi_w(0) - \int_0^{\hat{\tau}} Q_a(\sigma)\frac{\mathrm{d}\phi_{\mathrm{w}}(\hat{\tau}-\sigma)}{\mathrm{d}\sigma}\mathrm{d}\sigma\right), \\
\text{(A.2b)} \qquad T_\alpha &= \pi\rho_a b^2 \left[b\bar{a}\ddot{h} - Vb\left(\frac{1}{2} - \bar{a}\right)\dot{\alpha} - b^2\left(\frac{1}{8} + \bar{a}^2\right)\ddot{\alpha} - \frac{V^2}{\pi}\left(T_4 + T_{10}\right)\beta\right. \\
&\quad \left. + \frac{Vb}{\pi}\left(-T_1 + T_8 + (\bar{c} - \bar{a})T_4 - \frac{1}{2}T_{11}\right)\dot{\beta} + \frac{b^2}{\pi}\left(T_7 + (\bar{c} - \bar{a})T_1\right)\ddot{\beta}\right] \\
&\quad + 2\pi\rho_a V b^2\left(\bar{a} + \frac{1}{2}\right)\left(Q_a(\hat{\tau})\phi_w(0) - \int_0^{\hat{\tau}} Q_a(\sigma)\frac{\mathrm{d}\phi_{\mathrm{w}}(\hat{\tau}-\sigma)}{\mathrm{d}\sigma}\mathrm{d}\sigma\right), \\
\text{(A.2c)} \qquad T_\beta &= \pi\rho_a b^2 \left[\frac{b}{\pi}T_1\ddot{h} + \frac{Vb}{\pi}\left(2T_9 + T_1 - \left(\bar{a} - \frac{1}{2}\right)T_4\right)\dot{\alpha} - \frac{2b^2}{\pi}T_{13}\ddot{\alpha}\right. \\
&\quad \left. - \left(\frac{V}{\pi}\right)^2\left(T_5 - T_4T_{10}\right)\beta + \frac{Vb}{2\pi^2}T_4T_{11}\dot{\beta} + \left(\frac{b}{\pi}\right)^2 T_3\ddot{\beta}\right] \\
&\quad - \rho_a V b^2 T_{12}\left(Q_a(\hat{\tau})\phi_w(0) - \int_0^{\hat{\tau}} Q_a(\sigma)\frac{\mathrm{d}\phi_w(\hat{\tau}-\sigma)}{\mathrm{d}\sigma}\mathrm{d}\sigma\right).
\end{aligned}$$

In order to approximate the unsteady aerodynamics, we use the exponential approximation to the Theodorsen functions

$$\phi(\tau) = 1 - a_1\mathrm{e}^{-b_1\tau} - a_2\mathrm{e}^{-b_2\tau},$$

as introduced by Jones [16], and see [29] for a derivation and for how to define values of the coefficients $a_{1,2}$ and $b_{1,2}$. Then we introduce augmented variables

$$w_1(t) = \int_0^t Q_a\mathrm{e}^{-\mathrm{b}_1(\mathrm{t}-\sigma)}\mathrm{d}\sigma, \quad w_2(t) = \int_0^t Q_a\mathrm{e}^{-\mathrm{b}_2(\mathrm{t}-\sigma)}\mathrm{d}\sigma \tag{A.3}$$

to calculate the aerodynamic forces L, T_α T_β in terms of feedback from the structural motion, where

$$Q_a = \left(V\alpha + \dot{h} + b\left(\frac{1}{2} - \bar{a}\right)\dot{\alpha} + \frac{V}{\pi}T_{10}\beta + \frac{b}{2\pi}T_{11}\dot{\beta}\right).$$

If we define $X_s = [\zeta, \alpha, \beta]^\top$ for the structural variables and $w_p = [w_1, w_2]^\top$ for the augmented parametric variables, then the full coupled system can be written as

$$\begin{aligned}
\dot{X}_s &= \dot{X}_s, \\
M\ddot{X}_s &= -KX_s - C\dot{X}_s - D_w w_p, \\
\dot{w}_p &= E_q X_s + E_{qd}\dot{X}_s + E_w w_p,
\end{aligned} \tag{A.4}$$

where

$$M = \overline{M} - \eta M_{nc},\ K = \overline{K} - \eta(U/b)^2(K_{nc} + 0.5R_cS_{c1}),\ C = \overline{C} - \eta(U/b)(B_{nc} + 0.5R_cS_{c2}),$$
$$D_\omega = \eta(U/b)R_c\left[a_1b_1(U/b)^2 \quad a_2b_2(U/b)\right],\ E_q = (U/b)\left[S_{c1}; S_{c1}\right],\ E_{qd} = \left[S_{c2}; S_{c2}\right],$$
$$E_\omega = \begin{bmatrix} -b_1 & 0 \\ 0 & -b_2 \end{bmatrix}, \quad \eta = 1/\pi\mu, \quad \text{and} \quad \mu = m/\pi\rho_a b^2,$$
$$\boldsymbol{M}_{nc} = \begin{bmatrix} -\pi & \pi\bar{a} & T_1 \\ \pi\bar{a} & -\pi\left(1/8 + \bar{a}^2\right) & -2T_{13} \\ T_1 & -2T_{13} & T_3/\pi \end{bmatrix}, \qquad \boldsymbol{B}_{nc} = \begin{bmatrix} 0 & -\pi & T_4 \\ 0 & \pi(\bar{a} - 0.5) & -T_{16} \\ 0 & -T_{17} & -T_{19}/\pi \end{bmatrix},$$
$$\boldsymbol{R}_c = \begin{bmatrix} -2\pi \\ 2\pi(\bar{a} + 0.5) \\ -T_{12} \end{bmatrix}, \qquad \boldsymbol{K}_{nc} = \begin{bmatrix} 0 & 0 & 0 \\ 0 & 0 & -T_{15} \\ 0 & 0 & -T_{18}/\pi \end{bmatrix},$$
$$\boldsymbol{S}_{c1} = \begin{bmatrix} 0 & 1 & \dfrac{T_{10}}{\pi} \end{bmatrix}, \qquad \boldsymbol{S}_{c2} = \begin{bmatrix} 1 & 0.5 - \bar{a} & \dfrac{T_{11}}{2\pi} \end{bmatrix}$$

with all T_i constants given in [28].

Finally, transform the differential-integral equations (A.1) into the following system of first-order ODEs:

$$\text{(A.5)} \qquad \begin{bmatrix} \dot{X}_s \\ \ddot{X}_s \\ \dot{w}_{\mathrm{p}} \end{bmatrix} = \begin{bmatrix} \mathbf{0}_{3\times3} & \boldsymbol{I}_{3\times3} & \mathbf{0}_{3\times2} \\ -\boldsymbol{M}^{-1}\boldsymbol{K} & -\boldsymbol{M}^{-1}\boldsymbol{C} & -\boldsymbol{M}^{-1}\boldsymbol{D} \\ \boldsymbol{E}_q & \boldsymbol{E}_{qd} & \boldsymbol{E}_w \end{bmatrix} \begin{bmatrix} X_s \\ \dot{X}_s \\ w_{\mathrm{p}} \end{bmatrix} + \begin{bmatrix} \mathbf{0}_{3\times1} \\ -\boldsymbol{M}^{-1}\boldsymbol{F}(X_s) \\ \mathbf{0}_{2\times1} \end{bmatrix}.$$

The detailed physical parameters used in this study are given in Table 4. **AQ17**

For convenience, we also specify here the numerically evaluated matrices necessary to compute the normal form (2.12) at the BEB we have found at parameter values $\bar{U} = 0.64833$ and $\delta = 0.01$ rad. After numerical evaluation, we find

$$\mathbf{A} = [\mathbf{A}_1\ \mathbf{A}_2],$$

Table 4
Parameter definition

Physical parameters					
b	ω_h	ω_α	ω_β	ρ_a	m
0.3 m	50 rad/s	100 rad/s	0 rad/s	1.225 kg/mm^3	1.5 kg
a_1	a_2	b_1	b_2	$\xi_i,\ i = h,\alpha,\beta$	r
0.165	0.0455	0.335	0.3	2%	0.72
Dimensionless parameters					
$\bar{a}$	$\bar{c}$	$\bar{x}_\alpha$	$\bar{x}_\beta$	$\bar{r}_\alpha^2$	$\bar{r}_\beta^2$
−0.4	0.6	0.2	0.0125	0.25	0.00625

where

$$\mathbf{A}_1 = \begin{pmatrix} 0 & 0 & 0 \\ 0 & 0 & 0 \\ 0 & 0 & 0 \\ -2.9340e+03 & 2.3800e+03 & -31.8848 \\ 2.5143e+03 & -1.4569e+04 & -126.9591 \\ -1.5787e+03 & 3.9373e+04 & 119.8092 \\ 0 & 0 & 0 \\ 0 & 64.8330 & 35.6462 \end{pmatrix},$$

$$\mathbf{A}_2 = \begin{pmatrix} 1 & 0 & 0 & 0 & 0 \\ 0 & 1 & 0 & 0 & 0 \\ 0 & 0 & 1 & 0 & 0 \\ -4.1409 & -1.7578 & -0.2147 & -118.8655 & -29.0256 \\ 3.3583 & -8.2454 & -1.0773 & 157.7863 & 38.5297 \\ -3.2826 & 17.0083 & -1.9570 & -328.2203 & -80.1478 \\ 0 & 0 & 0 & 0 & 1 \\ 1 & 0.9000 & 0.1487 & -57.3753 & -22.3998 \end{pmatrix}$$

and the reset map related matrices are

$$\mathbf{C}^\top = \begin{pmatrix} 0 \\ 0 \\ 1 \\ 0 \\ 0 \\ 0 \\ 0 \\ 0 \end{pmatrix}, \ \mathbf{B} = (1+r) \begin{pmatrix} 0 \\ 0 \\ 0 \\ 0.0030 \\ -0.0774 \\ 1 \\ 0 \\ 0 \end{pmatrix}.$$

Appendix B. Derivation of normal form. We give here a constructive proof of Theorem 2.4, by specifying the specific transformations necessary to put a general n-dimensional impacting hybrid system undergoing a BEB with linearization (2.8) into the normal form (2.12).

Without loss of generality, we first set $\mu^* = 0$ in (2.8) and assume the sign convention that transition from an admissible to a virtual equilibrium occurs as μ increases through zero. Then, according to (2.8) the linearization around the admissible equilibrium $\bar{\mathbf{x}}$ for $\mu < 0$ with $H(\bar{\mathbf{x}}) > 0$ satisfies

$$\mathbf{A}(\bar{\mathbf{x}}-\mathbf{x}^*)+\mathbf{M}\mu=0,$$
$$\mathbf{C}(\bar{\mathbf{x}}-\mathbf{x}^*)+\mathbf{N}\mu=\eta,$$

where

$$\eta=-(\mathbf{C}\mathbf{A}^{-1}\mathbf{M}-\mathbf{N})\mu>0, \tag{B.1}$$

which implies $\mathbf{C}\mathbf{A}^{-1}\mathbf{M}-\mathbf{N}>0$.

Next, setting $\Delta\mathbf{x}=\bar{\mathbf{x}}-\mathbf{x}^*$, we arrive at

$$\begin{aligned}\tilde{F}(\mathbf{x},\mu)&=\mathbf{A}\Delta\mathbf{x}+\mathbf{M}\mu\\&=\mathbf{A}(\Delta\mathbf{x}+\mathbf{A}^{-1}\mathbf{M}\mu),\\\tilde{H}(\mathbf{x},\mu)&=\mathbf{C}(\Delta\mathbf{x}+\mathbf{A}^{-1}\mathbf{M}\mu)+(\mathbf{N}-\mathbf{C}\mathbf{A}^{-1}\mathbf{M})\mu.\end{aligned}$$

We can now rescale the problem by dividing by the positive scalar

$$|\mu|(\mathbf{C}\mathbf{A}^{-1}\mathbf{M}-\mathbf{N}). \tag{B.2}$$

Then we reorganize the system using a new state variable

$$\mathbf{y}=\frac{\Delta\mathbf{x}+\mathbf{A}^{-1}\mathbf{M}\mu}{|\mu|(\mathbf{C}\mathbf{A}^{-1}\mathbf{M}-\mathbf{N})},$$

under which the reset map (2.3) becomes a linear transform

$$\begin{aligned}\mathbf{y}^+&=\mathbf{y}^-+W(\mathbf{y}^-)v(\mathbf{y}^-)\\&=\mathbf{y}^--\mathbf{B}\mathbf{C}\mathbf{A}\mathbf{y}^-\\&=\mathbf{P}\mathbf{y}^-\end{aligned} \tag{B.3}$$

with

$$v(\mathbf{y}^-)=\mathcal{L}_F(H)(\mathbf{y}^-)=\mathbf{C}\mathbf{A}\mathbf{y}^- \text{ and discontinuity set } \tilde{H}(\mathbf{y},\hat{\mu}):=\mathbf{C}\mathbf{y}-\hat{\mu}=0,$$

where $\hat{\mu}=\operatorname{sign}(\mu)$, so that the the dynamics around the boundary equilibrium can be be fully understood by studying on the cases $\hat{\mu}\in\{-1,0,1\}$.

Accordingly, we redefine the incoming set as $\{\Sigma^-|v<0,H(\mathbf{y})=0\}$, the outgoing set $\{\Sigma^+|v>0,H(\mathbf{y})=0\}$, and the grazing set $\{\Sigma^0|v=0,H(\mathbf{y})=0\}$ on the discontinuity set $\{\Sigma|H(\mathbf{y})=0\}$, where $v=\mathcal{L}_F(H)(\mathbf{y})$. Thus, the reset map will map the points in Σ^- to Σ^+. The vector fields for their free flight and sticking motion are driven by respective vector fields

$$\tilde{F}(\mathbf{y},\hat{\mu})=\mathbf{A}\mathbf{y} \text{ and } F_s(\mathbf{y},\hat{\mu})=\mathbf{A}_s\mathbf{y}.$$

Furthermore, we note that the observing vector $\mathbf{C}$ can be transformed to a unit vector $\mathbf{e}_1^T$ by an additional coordinate transform, which also has the effect of redefining $\mathbf{A}$ and $\mathbf{B}$. Without loss of generality, consider a general unit observing vector $\mathbf{C}^\top\in\mathbb{R}^n$ (otherwise, we can normalize it). We also assume the nondegeneracy condition that $\mathbf{C}^\top$ is not tangent to the eigenspace of $\mathbf{A}$.

Then, in general, $\mathbf{C}^\top$ can be parameterized by $n-1$ independent parameters, via

$$\mathbf{C}^\top = \begin{bmatrix} \cos\theta_1 \prod_{i=2}^{n-1} \sin\theta_i \\ \sin\theta_1 \prod_{i=2}^{n-1} \sin\theta_i \\ \cos\theta_2 \prod_{i=3}^{n-1} \sin\theta_i \\ \vdots \\ \cos\theta_{n-2} \sin\theta_{n-1} \\ \cos\theta_{n-1} \end{bmatrix}. \tag{B.4}$$

To see this, observe the following:

1. $C_1^2 + C_2^2 = \prod_{i=2}^{n-1} \sin^2\theta_i$.
2. $C_1^2 + C_2^2 + C_3^2 = \prod_{i=3}^{n-1} \sin^2\theta_i$.
3. We can observe the form of remaining elements of $\mathbf{C}$ to easily conclude that $\sum_1^m C_i^2 = \prod_{i=m}^{n-1} \sin^2\theta_i$ for $2 \le m \le n-1$.

Therefore, we have

$$\mathrm{norm}(\mathbf{C}) = \sum_{i=1}^{n} C_i^2 = \sum_{i=1}^{n-1} C_i^2 + \cos^2\theta_{n-1} = 1.$$

The kernel space $\mathbf{C}$ is given by

$$\mathrm{Ker}(\mathbf{C}) = \{\mathbf{v} \in \mathbb{R}^n \mid \mathbf{C}\mathbf{v} = 0\},$$

and we can find an orthogonal basis for this subspace so that

$$\mathrm{Ker}(\mathbf{C}) = \mathrm{span}\{\mathbf{e}_\mathrm{k}^2, \dots, \mathbf{e}_\mathrm{k}^n\},$$

and from (2.9) we know that the vector $\mathbf{B}$ is in this kernel. So we can write

$$\mathbf{B} = b_2\mathbf{e}_\mathrm{k}^2 + \cdots + b_\mathrm{n}\mathbf{e}_\mathrm{k}^n, \text{ where } b_i = \langle \mathbf{B}, \mathbf{e}_\mathrm{k}^i \rangle,\ i = 2, \dots, n.$$

Furthermore, let us define a transformation matrix

$$\mathbf{T} = [\mathbf{C}^\top, \mathbf{e}_\mathrm{k}^2, \mathbf{e}_\mathrm{k}^3]. \tag{B.5}$$

Under such a transformation and rescaled time $\mathrm{d}t = \mathrm{d}\tau/s$, $s \in \mathbb{R}^+$, the system is converted to one with corresponding matrices

$$\hat{\mathbf{A}} = \mathbf{T}^{-1}\frac{\mathbf{A}}{s}\mathbf{T},\ \hat{\mathbf{B}} = \mathbf{T}^{-1}\mathbf{B} = \begin{bmatrix} 0 \\ b_2 \\ \vdots \\ b_n \end{bmatrix},\ \hat{\mathbf{C}} = \mathbf{C}\mathbf{T} = \mathbf{e}_1, \mathbf{P} = \mathbf{I} - \hat{\mathbf{B}}\hat{\mathbf{C}}\hat{\mathbf{A}}. \tag{B.6}$$

Compared to (2.10), it can be easily checked that $\hat{\mathbf{A}}_s = \mathbf{T}^{-1}\frac{\mathbf{A}_s}{s}\mathbf{T}$.

Appendix C. Reduced description in the three-dimensional case. For the three-dimensional case, it is possible to derive the conditions (3.7b) explicitly. Following (3.9), the minimal parameter space to define the matrices $\hat{\mathbf{A}}$ and $\hat{\mathbf{B}}$ is

$$\Lambda = \{\lambda_1, \lambda_2, \lambda_3, b_2, b_3, \theta, \varphi\}. \tag{C.1}$$

Furthermore, without loss of generality, provided $\lambda_3 \neq 0$, we can rescale time, for example, to assume $\lambda_3 = \pm 1$. We now derive explicit equations for $p(t)$ and velocity v in terms of these two parameters in each of the two cases (C.2) and (C.5).

C.1. Case I. If we denote $\Delta_{ij} = \lambda_i - \lambda_j$, then it is straightforward to find coordinate transformations to express $\hat{\mathbf{A}}$ and $\hat{\mathbf{B}}$ in terms of the parameter set (C.1). We find

$$\hat{\mathbf{A}} = \begin{bmatrix} a_{11} & a_{12} & a_{13} \\ a_{21} & a_{22} & a_{23} \\ a_{31} & a_{32} & a_{33} \end{bmatrix}, \quad \hat{\mathbf{B}} = \begin{bmatrix} 0 \\ b_2 \\ b_3 \end{bmatrix}, \quad \hat{\mathbf{C}}^\top = \begin{bmatrix} 1 \\ 0 \\ 0 \end{bmatrix} \tag{C.2a}$$

and

$$\mathbf{P} = \begin{bmatrix} 1 & 0 & 0 \\ p_{21} & p_{22} & \frac{b_2 \sin(2\theta)}{2} \sin\varphi \Delta_{21} \\ p_{31} & p_{32} & 1 + \frac{b_3 \sin(2\theta)}{2} \sin\varphi \Delta_{21} \end{bmatrix}, \tag{C.2b}$$

where

$$a_{11} = \Delta_{12} \sin^2\varphi \cos^2\theta + \Delta_{32} \cos^2\varphi + \lambda_2,\ a_{12} = \sin\varphi\cos\varphi(\Delta_{12}\cos^2\theta + \Delta_{23}),$$

$$a_{13} = \frac{\sin(2\theta)}{2}\sin\varphi\Delta_{21},\ a_{22} = (\Delta_{12}\cos^2\theta + \Delta_{23})\cos^2\varphi + \lambda_3,\ a_{23} = \frac{\sin(2\theta)}{2}\cos\varphi\Delta_{21},$$

$$a_{33} = \Delta_{21}\cos^2\theta + \lambda_1,\ a_{21} = a_{12},\ a_{31} = a_{13}, a_{32} = a_{21},$$

and

$$p_{21} = -b_2(\Delta_{12}\sin^2\varphi\cos^2\theta + \Delta_{32}\cos^2\varphi + \lambda_2),\ p_{22} = 1 - b_2\sin\varphi\cos\varphi(\Delta_{12}\cos^2\theta + \Delta_{23}),$$

$$p_{31} = -b_3(\Delta_{12}\sin^2\varphi\cos^2\theta + \Delta_{32}\cos^2\varphi + \lambda_2),\ p_{32} = -b_3\sin\varphi\cos\varphi(\Delta_{12}\cos^2\theta + \Delta_{23}).$$

Thus, by taking an exponential of the appropriate diagonal matrix and transforming back, **AQ18**
we can write the existence condition (3.7b) explicitly as

$$\begin{aligned} p(\Lambda, t) = &-1 + h_{11}\,\mathrm{e}^{(\lambda_1+\lambda_2+\lambda_3)t} + h_{12}\,\mathrm{e}^{(\lambda_1+\lambda_2)t} + h_{13}\,\mathrm{e}^{(\lambda_2+\lambda_3)t} \\ &- (1 + 2h_{11} + h_{12} + h_{13})\,\mathrm{e}^{(\lambda_1+\lambda_3)t} + (1 + h_{11} + h_{12})\,\mathrm{e}^{\lambda_3 t} \\ &- (h_{11} + h_{12} + h_{13})\,\mathrm{e}^{\lambda_2 t} + (1 + h_{11} + h_{13})\,\mathrm{e}^{\lambda_1 t} = 0, \end{aligned} \tag{C.3}$$

where

$$\begin{aligned}
h_{11} =& 1 - b_2(\lambda_1 \cos^2\theta + \lambda_2 \sin^2\theta - \lambda_3) \sin\varphi \cos\varphi \\
& + b_3(\lambda_1 - \lambda_2) \sin\theta \cos\theta \sin\varphi, \\
h_{12} =& -1 + b_2(\lambda_1 \cos^2\theta + \lambda_2 \sin^2\theta) \sin\varphi \cos\varphi \\
& - b_3(\lambda_1 - \lambda_2) \sin\theta \cos\theta \sin\varphi, \\
h_{13} =& -1 + b_2(\lambda_2 \sin^2\theta - \lambda_3) \sin\varphi \cos\varphi \\
& + b_3\lambda_2 \sin\theta \cos\theta \sin\varphi.
\end{aligned}$$

Combining the (4.2) and (3.3), we can also write down the expression that determines the direction of bifurcation,

$$\begin{aligned}
\hat{v}(\Lambda, T) =& k_{11}\,\mathrm{e}^{(\lambda_1+\lambda_2)t} + k_{12}\,\mathrm{e}^{(\lambda_1+\lambda_3)t} + k_{13}\,\mathrm{e}^{(\lambda_2+\lambda_3)t} \\
& + (k_{11} - k_{10})\,\mathrm{e}^{\lambda_3 t} + (k_{12} - k_{10})\,\mathrm{e}^{\lambda_2 t} + (k_{13} - k_{10})\,\mathrm{e}^{\lambda_1 t} + k_{10},
\end{aligned} \tag{C.4}$$

where

$$\begin{aligned}
k_{10} =& (\lambda_1 \cos^2\theta + \lambda_2 \sin^2\theta) \sin^2\varphi + \lambda_3 \cos^2\varphi, \\
k_{11} =& \lambda_3 \cos^2\varphi - b_2(\lambda_1 \cos^2\theta + \lambda_2 \sin^2\theta)\lambda_3 \cos\varphi \sin\varphi \\
& + b_3(\lambda_1 \cos^2\varphi - \lambda_2 \cos^2\varphi)\lambda_3 \sin\theta \cos\theta \sin\varphi, \\
k_{12} =& \lambda_2 \sin^2\theta \sin^2\varphi + b_2\lambda_2\lambda_3 \sin^2\theta \sin\varphi \cos\varphi \\
& + b_3(\lambda_1 \sin^2\varphi + \lambda_3 \cos^2\varphi)\lambda_2 \sin\theta \cos\theta \sin\varphi, \\
k_{13} =& \lambda_1 \cos^2\theta \sin^2\varphi + b_2\lambda_1\lambda_3 \cos^2\theta \sin\varphi \cos\varphi \\
& - b_3(\lambda_2 \sin^2\varphi + \lambda_3 \cos^2\varphi)\lambda_1 \sin\theta \cos\theta \sin\varphi.\lambda_3 \cos^2\varphi.
\end{aligned}$$

AQ19

C.2. Case II.

Proceeding similarly for the focus case, we find

$$\mathbf{A} = \begin{bmatrix} (\lambda_3 - \alpha)\cos^2\varphi + \alpha & \sin\varphi\cos\varphi(\alpha - \lambda_3) & \beta\sin\varphi \\ \sin\varphi\cos\varphi(\alpha - \lambda_3) & (\alpha - \lambda_3)\cos^2\varphi + \lambda_3 & \beta\cos\varphi \\ -\beta\sin\varphi & -\beta\cos\varphi & \alpha \end{bmatrix}, \hat{\mathbf{B}} = \begin{bmatrix} 0 \\ b_2 \\ b_3 \end{bmatrix}, \hat{\mathbf{C}}^\top = \begin{bmatrix} 1 \\ 0 \\ 0 \end{bmatrix}, \tag{C.5a}$$

and

$$\mathbf{P} = \begin{bmatrix} 1 & 0 & 0 \\ (\cos^2\varphi(\alpha - \lambda_3) - \alpha)b_2 & 1 - b_2(\alpha - \lambda_3)\cos\varphi\sin\varphi & -b_2\beta\sin\varphi \\ (\cos^2\varphi(\alpha - \lambda_3) - \alpha)b_3 & -b_3(\alpha - \lambda_3)\cos\varphi\sin\varphi & 1 - b_3\beta\sin\varphi \end{bmatrix}. \tag{C.5b}$$

Then, the existence condition can be explicitly written as

$$\begin{aligned}
p(\Lambda, t) =& h_{21}\,\mathrm{e}^{(2\alpha+\lambda_3)t} + h_{22}\,\mathrm{e}^{(\alpha+\lambda_3)t}\cos(\beta t) + h_{23}\,\mathrm{e}^{(\alpha+\lambda_3)t}\sin(\beta t) \\
& - (1 + 2h_{21} - h_{22})\,\mathrm{e}^{2\alpha t} + (2 + 2h_{21} + h_{22})\,\mathrm{e}^{\alpha t}\cos(\beta t) \\
& - h_{23}\,\mathrm{e}^{\alpha t}\sin(\beta t) - (h_{21} + h_{22})\,\mathrm{e}^{\lambda_3 t} - 1 = 0,
\end{aligned} \tag{C.6}$$

where

$$h_{21} = 1 - [b_2(\alpha - \lambda_3)\cos\varphi + b_3\beta]\sin\varphi,$$
$$h_{22} = -2 + [b_2(\alpha - 2\lambda_3)\cos\varphi + b_3\beta]\sin\varphi,$$
$$h_{23} = -(b_2\beta\cos\varphi - b_3\alpha)\sin\varphi.$$

Combining the (3.3), we can write down the expression that determines the direction of bifurcation,

$$\begin{aligned}\hat{v}(\Lambda, T) = k_{21}\,\mathrm{e}^{(\alpha+\lambda_3)t}\cos(\beta t) + k_{22}\,\mathrm{e}^{(\alpha+\lambda_3)t}\sin(\beta t) + (k_{20} - k_{21})\,\mathrm{e}^{2\alpha t} \\ + (k_{21} - 2k_{20})\,\mathrm{e}^{\alpha t}\cos(\beta t) - k_{22}\,\mathrm{e}^{\alpha t}\sin(\beta t) - k_{21}\,\mathrm{e}^{\lambda_3 t} + k_{20},\end{aligned} \tag{C.7}$$

where

$$k_{20} = \alpha\sin^2\varphi + \lambda_3\cos^2\varphi,$$
$$k_{21} = (b_2\alpha + b_3\beta\cos\varphi)\lambda_3\cos\varphi\sin\varphi + \alpha\sin^2\varphi,$$
$$k_{22} = [\beta\sin\varphi + b_2\beta\lambda_3\cos\varphi - b_3\left(\alpha\lambda_3\cos^2\varphi + (\alpha^2+\beta^2)\sin^2\varphi\right)]\sin\varphi.$$

Appendix D. General analytic form for $p(t)$. Let $\mathbf{K}(t) = \mathbf{P}\mathrm{e}^{\mathbf{A}t} - \mathbf{I}$, so that $p(t) = \det(\mathbf{K}(t))$. We know $p(0) = 0$, so we can expand this analytic function around $t = 0$. We can write

$$\mathrm{e}^{\mathbf{A}t} = \mathbf{I} + \mathbf{A}t + \frac{1}{2!}\mathbf{A}^2t^2 + \sum_{l=3}^{\infty}\frac{\mathbf{A}^l}{l!} \tag{D.1}$$

and

$$\det(\mathbf{K}) = |\mathbf{P} - \mathbf{I} + \mathbf{PA}t + \frac{1}{2!}\mathbf{PA^2}t^2 + \sum_{l=3}^{\infty}\frac{\mathbf{A}^l}{l!}|.$$

Now we can appeal to the following standard result from linear algebra [26].

Lemma D.1. *Suppose* $\mathbf{Q}$ *and* $\mathbf{K}$ *are invertible* $n \times n$ *matrices, then*

$$\det(\mathbf{QK}) = \det(\mathbf{Q})\det(\mathbf{K}),$$

and hence

$$\det((\mathbf{K})) = \det(\mathbf{Q}^{-1}\mathbf{KQ}).$$

According to Lemma D.1, we can split $p(t)$ into

$$p(t) = \det(\mathbf{P})\det\left(\mathbf{I} - \mathbf{P^{-1}} + \mathbf{A}t + \frac{1}{2!}\mathbf{A^2}t^2 + \sum_{l=3}^{\infty}\frac{\mathbf{A}^lt^l}{l!}\right).$$

Further let $\mathcal{P}(t)$ be the polynomial $p(t)/\det(\mathbf{P})$, and write

$$\mathcal{P}(t) = \sum_{k=0}^{\infty}p_kt^k, \tag{D.2}$$

where we know that $\det(\mathbf{P}) = -r$. Now let us find information about the coefficients p_k. The following result is useful.

Definition D.2. [19] *Let α and β be integer sequences of length $1 \le m \le n$ chosen from $1, \ldots, n$:*
- $\mathbf{A}[\alpha|\beta]$ *(square brackets) is the $m \times m$ submatrix of $\mathbf{A}$ lying in rows α and columns β;*
- $\mathbf{B}(\alpha|\beta)$ *(round brackets) is the $(n-m)\times(n-m)$ submatrix of $\mathbf{B}$ lying in rows complementary to α and columns complementary to β.*

Lemma D.3. [19] *For two $n \times n$ matrices $\mathbf{A}$ and $\mathbf{B}$, the determinant of their sum is given by*

$$\det(\mathbf{A}+\mathbf{B}) = \sum_{m=1}^{n} \sum_{\alpha,\beta} (-1)^{s(\alpha)+s(\beta)} \det(\mathbf{A}[\alpha|\beta]) \det(\mathbf{B}(\alpha|\beta)), \tag{D.3}$$

where m denotes the number of rows and columns extracted from $\mathbf{A}$. For a particular m, the inner sum is over all strictly increasing integer sequences α and β of length m chosen from $1, \ldots, n$, and $s(\alpha)/s(\beta)$ is the sum of integers in α/β.

Lemma D.4. *Consider a matrix polynomial*

$$\mathbf{Z}(t) = \sum_{i=0}^{n} \mathbf{M}_i t^i,$$

where $\mathbf{M}_i$ are constant $n \times n$ matrices such that the determinant of $\mathbf{M}_i t$ is also a polynomial of t up to highest order t^{n^2}. According to Laplace expansion [26], we know the $\det(\mathbf{Z})$ is linearly dependent on every column of every elementary matrix $\mathbf{M}_i$. If we define a sequence

$$S = [s_0, s_1, \ldots, s_n],$$

where s_i denotes the number of elements from $\mathbf{M}_i$, which take part in the product term of the Laplace expansion. Obviously, $0 \le s_i \le n$ and $\sum s_i = n$; also, each s_i should be from different columns and rows of $\mathbf{M}_i$. We define $\delta(s_i)$ as an index set of integer number s_i, indicating column index of the elements $M_i^{j,k}$ in the Laplace expansion term. Then we can write

$$\det(\mathbf{Z}) = \sum_{S} (-1)^{\Gamma(S)} \left(\prod_{i=0}^{n} \det(\mathbf{M}_i[\delta(s_i)|\sigma(s_i)]) \cdot t^{(i\, s_i)} \right).$$

Now, applying Lemma D.4, we substitute

$$\mathbf{M}_0 = \mathbf{I} - \mathbf{P}^{-1} = -\frac{1}{r}\mathbf{BCA}, \quad \mathbf{M}_i = \frac{\mathbf{A}^i}{i!},$$

and the order k_S of every expansion term with sequence S is $k_S = \sum_{i=1} i s_i$. We observe that $\operatorname{rank}(\mathbf{M}_0) = 1$, and the only nonzero eigenvalue $-\frac{1}{r}\mathbf{CAB}$. Thus, for all terms in the Laplace expansion with $s_0 > 1$, we have that $k_S \le n-2$ will be zero. To get all terms with $k_S \le n$ under the condition $s_0 \le 1$, the only sequences leading to possible nonzero terms are

$$S_1 = [0, n, 0, \ldots, 0],\ S_2 = [1, n-1, 0, \ldots, 0], \text{ and } S_3 = [1, n-2, 1, 0, \cdots, 0].$$

Then, by Lemma D.4, the following hold:

1. For S_1, the corresponding term is

$$\det(\mathbf{M}_1)t^n.$$

2. For S_2, the corresponding term is $\sum_{i=1}^{n}(-1)^{i+j}\mathbf{M}_0^{i,j}\,\mathrm{adj}(\mathbf{M}_1^{i,j})t^{n-1}$.
3. For S_3, the corresponding term is $(\mathrm{trace}(\mathbf{M}_0)\frac{\det(\mathbf{M}_1)}{2})t^n$.

The coefficient the t^{n-1} term derived from S_2 can be shown to be zero, because (i) $\mathbf{M}_0$'s row space is just expanded by $\mathbf{CA}$, and (ii) from condition (2.9) $\mathbf{CB} = 0$. Finally, we get the conclusion that the first $n-1$ terms of $\mathcal{P}$ are zero. Thus, the n_{th}-order term is the leading order of $\mathcal{P}(t)$, which can be calculated by summing terms from S_1 and S_3, **AQ20**

$$\det(\mathbf{M}_1)(1+\frac{\mathrm{trace}(\mathbf{M}_0)}{2})t^n.$$

Therefore, by multiplying the above with $\det(\mathbf{P})$, the leading order for the $p(t)$ is

$$-\frac{1}{2}(r-1)\det(\mathbf{A})t^n. \tag{D.4}$$

Acknowledgments. The authors thank Mike Jeffrey and Nick Lieven for helpful conversations.

REFERENCES

[1] E. L. Allgower and K. Georg, *Introduction to Numerical Continuation Methods*, Classics Appl. Math. 45, SIAM, Philadelphia, 2003, https://doi.org/10.1137/1.9780898719154.

[2] I. Belykh, R. Kuske, M. Porfiri, and D. Simpson, *Beyond the Bristol book: Advances and perspectives in non-smooth dynamics and applications*, Chaos, 33 (2023), 010402.

[3] V. Carmona and F. Fernández-Sánchez, *Integral characterization for Poincaré half-maps in planar linear systems*, J. Differential Equations, 305 (2021), pp. 319–346, https://doi.org/10.1016/j.jde.2021.10.010.

[4] V. Carmona, F. Fernández-Sánchez, and D. D. Novaes, *Uniform upper bound for the number of limit cycles of planar piecewise linear differential systems with two zones separated by a straight line*, Appl. Math. Lett., 137 (2023), 108501, https://doi.org/10.1016/j.aml.2022.108501.

[5] V. Carmona, F. Fernández-Sánchez, and D. D. Novaes, *Uniqueness and stability of limit cycles in planar piecewise linear differential systems without sliding region*, Commun. Nonlinear Sci. Numer. Simul., 123 (2023), 107257, https://doi.org/10.1016/j.cnsns.2023.107257.

[6] V. Carmona, E. Freire, E. Ponce, and F. Torres, *Bifurcation of invariant cones in piecewise linear homogeneous systems*, Internat. J. Bifur. Chaos, 15 (2005), pp. 2469–2484, https://doi.org/10.1142/S0218127405013423.

[7] M. di Bernardo, C. Budd, A. Champneys, and P. Kowalczyk, *Piecewise-Smooth Dynamical Systems: Theory and Applications*, Appl. Math. Sci., Springer, New York, 2008, https://doi.org/10.1007/978-1-84628-708-4.

[8] M. di Bernardo, A. Nordmark, and G. Olivar, *Discontinuity-induced bifurcations of equilibria in piecewise-smooth and impacting dynamical systems*, Phys. D, 237 (2008), pp. 119–136, https://doi.org/10.1016/j.physd.2007.08.008.

[9] T. Dossogne, J. P. Noël, C. Grappasonni, G. Kerschen, B. Peeters, J. Debille, M. Vaes, and J. Schoukens, *Nonlinear ground vibration identification of an F-16 aircraft—Part II: Understanding nonlinear behaviour in aerospace structures using sine-sweep testing*, in Proceedings of the International Forum on Aeroelasticity and Structural Dynamics, IFASD 2015, 2015, pp. 1–19.

[10] M. H. Fredriksson and A. B. Nordmark, *On normal form calculations in impact oscillators*, Proc. A, 456 (2000), pp. 315–329, https://doi.org/10.1098/rspa.2000.0519.

[11] E. Freire, E. Ponce, and F. Torres, *Hopf-like bifurcations in planar piecewise linear systems*, Publ. Mat., 41 (2011), pp. 135–148, https://doi.org/10.5565/publmat4119708. **AQ14**

[12] M. S. Heiman, P. J. Sherman, and A. K. Bajaj, *On the dynamics and stability of an inclined impact pair*, J. Sound Vib., 114 (1987), pp. 535–547, https://doi.org/10.1016/S0022-460X(87)80022-6.

[13] C. Hős and A. Champneys, *Grazing bifurcations and chatter in a pressure relief valve model*, Phys. D, 241 (2012), pp. 2068–2076.

[14] M. Jeffery, *Hidden Dynamics: The Mathematics of Switches, Decisions and Other Discontinuous Behaviour*, Springer, New York, 2018.

[15] M. R. Jeffrey, T. I. Seidman, M. A. Teixeira, and V. I. Utkin, *Into higher dimensions for nonsmooth dynamical systems*, Phys. D, 434 (2022), 133222, https://doi.org/10.1016/j.physd.2022.133222.

[16] R. T. Jones, *Operational Treatment of the Non-Uniform Lift Theory in Airplane Dynamics*, https://digital.library.unt.edu/ark:/67531/metadc54463/, 1938.

[17] Y. A. Kuznetsov, *Elements of Applied Bifurcation Theory*, 2nd ed., Appl. Math. Sci. 112, Springer, Berlin, 1998.

[18] R. Leine and H. Nijmeijer, *Dynamics and Bifurcations of Non-Smooth Mechanical Systems*, Springer, New York, 2004.

[19] M. Marcus, *Determinants of sums*, College Math. J., 21 (1990), pp. 130–135, https://doi.org/10.1080/07468342.1990.11973297.

[20] A. B. Nordmark, *Existence of periodic orbits in grazing bifurcations of impacting mechanical oscillators*, Nonlinearity, 14 (2001), pp. 1517–1542, https://doi.org/10.1088/0951-7715/14/6/306.

[21] A. B. Nordmark and P. T. Piiroinen, *Simulation and stability analysis of impacting systems with complete chattering*, Nonlinear Dynam., 58 (2009), pp. 85–106, https://doi.org/10.1007/s11071-008-9463-y.

[22] R. Seydel, *Practical Bifurcation and Stability Analysis*, 3rd ed., Springer, New York, 2010.

[23] D. Simpson, *A compendium of Hopf-like bifurcations in piecewise-smooth dynamical systems*, Phys. Lett. A, 382 (2018), pp. 2439–2444, https://doi.org/10.1016/j.physleta.2018.06.004.

[24] D. Simpson, *Twenty Hopf-like bifurcations in piecewise-smooth dynamical systems*, Phys. Rep., 970 (2022), pp. 1–80, https://doi.org/10.1016/j.physrep.2022.04.007.

[25] D. Simpson and J. Meiss, *Aspects of bifurcation theory for piecewise-smooth, continuous systems*, Phys. D, 241 (2012), pp. 1861–1868, https://doi.org/10.1016/j.physd.2011.05.002.

[26] G. Strang, *Introduction to Linear Algebra*, 5th ed., Cambridge University Press, Cambridge, 2021.

[27] H. Tang, A. R. Champneys, and N. Lieven, *Bifurcation Analysis of an Airfoil Model with Freeplay*, in preparation, 2023. **AQ15**

[28] Theodorsen, *Report no.* 496*, general theory of aerodynamic instability and the mechanism of flutter*, J. Franklin Inst., 219 (1935), pp. 766–767, https://doi.org/10.1016/S0016-0032(35)92022-1.

[29] J. Wright and J. Cooper, *Introduction to Aircraft Aeroelasticity and Loads*, Aerosp. Ser., Wiley, New York, 2008.